Aerosol optical properties over Europe: an evaluation of the AQMEII Phase 3 simulations against satellite observations

Laura Palacios-Peña[1], Pedro Jiménez-Guerrero[1], Rocío Baró[1], Alessandra Balzarini[2],
Roberto Bianconi[3], Gabriele Curci[4,5], Tony Christian Landi[6], Guido Pirovano[2], Marje Prank[7,8],
Angelo Riccio[9], Paolo Tuccella[4,5], and Stefano Galmarini[10]

[1]Physics of the Earth, Department of Physics, Regional Campus of International Excellence (Campus Mare Nostrum), University of Murcia (UMU-MAR), 30100 Murcia, Spain
[2]Ricerca sul Sistema Energetico (RSE SpA), Milano, Italy
[3]Enviroware srl, Concorezzo, MB, Italy
[4]CETEMPS, University of L'Aquila, Italy
[5]Dept. Physical and Chemical Sciences, University of L'Aquila, Italy
[6]CNR - Institute for Atmospheric Sciences and Climate, Bologna, Italy
[7]Finnish Meteorological Institute, Atmospheric Composition Research Unit, Helsinki, Finland
[8]Cornell University, Atmospheric and Earth Sciences, Ithaca, NY, USA
[9]University Parthenope of Naples, Dept. of Science and Technology, Napoli, Italy
[10]European Commission, Joint Research Centre (JRC), Directorate for Energy, Transport and Climate, Air and Climate Unit, Ispra (VA), Italy

Correspondence to: Pedro Jiménez-Guerrero (pedro.jimenezguerrero@um.es)

Abstract. The main uncertainties in estimates of changes in the Earth's energy budget are related to the role of atmospheric aerosols. These changes are caused mainly by aerosol-radiation (ARI) and aerosol-cloud interactions (ACI), which heavily depend on aerosol properties. From the 1980s, many international modelling initiatives have studied atmospheric aerosols and their climate effects. Phase 3 of the Air Quality Model Evaluation International Initiative (AQMEII) focuses on evaluating and

5 intercomparing regional and linked global/regional modelling systems by collaborating with the Task Force on the Hemispheric Transport of Air Pollution Phase 2 (HTAP2) initiative. Within this framework, the main aim of this work was to evaluate the representation of aerosol optical depth (AOD) and the Ångström exponent (AE) by the AQMEII Phase 3 simulations over Europe. The evaluation was made using satellite data from the Moderate Resolution Imaging Spectroradiometer (MODIS) sensors on board the Terra and Aqua platforms. The results indicated that the skills of AQMEII simulations in the AOD

10 representation produced fewer errors than in the AE. Regardless of the models and emissions used, models were skilful at representing the low and medium AOD values observed (below 0.5). However, high values (close to 1.0) were underestimated for biomass burning episodes, and were overestimated for desert dust contributions, related mainly to emission and boundary conditions. Despite this behaviour, the spatial and temporal variability of this variable was well-represented by all the models. Generally, the AE evaluation showed more serious errors than the AOD evaluation. Moreover, the observed variability of this

15 parameter was strongly underestimated in all the simulations.

Atmospheric
Chemistry
and Physics
Discussions

1 Introduction

The Fifth Assessment Report (AR5) of the Intergovernmental Panel of Climate Change (IPCC) ascribes the gravest uncertainty to estimate and interpret changes to the Earth's energy budget to aerosol and clouds. Atmospheric aerosols produce these changes mainly by two different ways: influencing the Earth's radiation, the so-called aerosol-radiation interactions (ARI); modifying clouds and precipitation, the so-called aerosol-clouds interactions (ACI), which also increase uncertainty due to clouds (Boucher et al., 2013).

ARI and ACI depend on the optical properties of atmospheric aerosols along with their atmospheric distribution and hygroscopicity, and their ability to act as cloud condensation nuclei (CCN) and ice nuclei (IN). All these properties are highly variable on space and time scales due to aerosol particles' short-lived, non-uniform emissions, and the dependence of sinks on meteorology (Boucher et al., 2013; Randall et al., 2007). Thus the determination of atmospheric aerosol properties, by a complex interplay between their sources, atmospheric transformation processes and their removal from the atmosphere (Boucher et al., 2013) plays a part in the gravest uncertainty of aerosol effects on the Earth's climate.

It was in the 1980s when the atmospheric science community began to pay increasing attention to the atmospheric aerosol subject (Fuzzi et al., 2015). Since then, major efforts have been made to acquire better knowledge of atmospheric aerosol properties and their interactions with the Earth's climate to reduce the above-mentioned grave uncertainty. Many regional field measurement campaigns have taken place; e.g., the Integrated Campaign for Aerosols, Gases and Radiation Budget (Moorthy et al., 2008, ICARB); the Megacity Impact on Regional and Global Environments field experiment (Paredes-Miranda et al., 2009, MILAGRO); the Integrated Project on Aerosol Cloud Climate and Air Quality interactions (Kulmala et al., 2011, EU-CAARI); Aerosol, Radiation, and Cloud Processes affecting Arctic Climate (Warneke et al., 2010, ARCPAC); among many others (Boucher et al., 2013). Moreover, global long-term aerosol measurements are taken by surface networks, such as Global Atmosphere Watch (Ogren, 2011, GAW), Aerosol Robotic Network (Holben et al., 1998, AERONET), the European Monitoring and Evaluation Programme (Tørseth et al., 2012, EMEP) or by satellite sensors, such as the Moderate Resolution Imaging Spectroradiometer (Remer et al., 2005, MODIS) or the Cloud-Aerosol Lidar and Infrared Pathfinder Satellite Observation (Winker et al., 2003, CALIPSO) among many other base measurements, base networks and instruments on board satellites (Boucher et al., 2013).

Measurements provide incomplete sampling, but can be combined with information from global and regional aerosol models. There are a number of international initiatives that study, among other climate issues, atmospheric aerosols and their climate effects. Some examples are the Aerosol Comparisons between Observations and Models project, now in their Phase II (Schulz et al., 2009, AEROCOM-II), the Coupled Model Intercomparison Project, now in Phase 6 (Eyring et al., 2016, CMIP6), the Chemistry-Climate Model Initiative (Eyring et al., 2013, CCMI) or the Aerosol and Chemistry Model Intercomparison Project (Collins et al., 2016, AerChemMIP). Among these initiatives and many others, the primary purpose of the Air Quality Model Evaluation International Initiative (Rao et al., 2011, AQMEII) is to coordinate international efforts in scientific research on regional air quality model evaluations across the modelling communities of North America and Europe.

AQMEII Phase 1 (Galmarini et al., 2012) focused on developing general model-to-model and model-to-observation evaluation methodologies, Phase 2 (Galmarini et al., 2015) on simulating aerosol/climate feedbacks with online coupled modelling systems. As part of this Phase 2, some studies have evaluated aerosol properties and their effects on the climate system. Balzarini et al. (2015) analysed online model sensitivity to the chemical mechanisms of WRF-Chem in reproducing aerosol

5   properties, and found that although different chemical mechanisms give different Aerosol Optical Depths (AOD), the latter was underestimated. Forkel et al. (2015) found pronounced feedback effects, such as a reduction in seasonal mean solar radiation of $20\,Wm^{-3}$ and temperature of $0.25°$ in the summer of 2010 when ARI were taken into account. High aerosol concentrations resulted in a 10-30% decreased precipitation and low concentrations in very low cloud droplet numbers (5-100 droplets cm^{-1}) and a 50-70% lower cloud liquid water, which led to an increase in downward solar radiation of almost 50% when ACI were

10   taken into account. Makar et al. (2015) evaluated the effect on chemistry due to feedback between aerosol and meteorology. In this study, ACI were usually found to have a stronger effect on the predictions of ozone, particulate matter and other species, and also on the atmospheric transport and chemistry of large emitting sources such as plumes from forest fires and large cities. A work similar is that of Wang et al. (2015), in which a multi-model assessment of major column abundances of gases, radiation, aerosol and cloud variables was made using available satellite data. The evaluation results showed an excellent agreement

15   between all the simulations and satellite-derived radiation variables, as well as precipitable water vapour. Other aerosol-/cloud-related variables, such as AOD, cloud optical thickness, cloud liquid water path, CCN and cloud droplet number concentration were moderately to largely underestimated by most simulations due to the underestimations of aerosol loadings. They also indicated grave uncertainties associated with the current model treatments of ACI.

Moreover, and through the AQMEII Phase 2, the working group 2 of the COST Action ES1004 EuMetChem (European

20   framework for online integrated air quality and meteorology modelling, http://www.eumetchem.info/) investigated the importance of different processes and feedbacks in online coupled chemistry-meteorology/climate models for air quality simulations and weather predictions. As part of this initiative, an important aerosol load episode, the Russian wildfires in 2010, was investigated. Some results indicated that the inclusion of ARI led to a drop of between 10 and $100\,Wm^{-2}$ of the average downward shortwave radiation on the ground and an almost $1°$ in the mean temperature (Forkel et al., 2016; Toll et al., 2015a). During the

25   same episode, Baró et al. (2017) found a reduction in the 10-metre wind speed of $0.2\,ms^{-1}$ (10%) since presence of biomass burning implied a reduction in shortwave downwelling radiation on the surface which, in turn, led to a reduction in the 2-metre temperature, and thus a reduction in the turbulence flux, and developed a stabler planetary boundary layer. Kong et al. (2015) and Palacios-Peña et al. (2017b) evaluated the observation of the inclusion effects of ARI and ACI for this wildfires episode and a desert dust outbreak. The results showed that a minor, but significant, improvement was observed when ARI and ACI

30   were taken into account.

In AQMEII Phase 3, to which this work is a contribution, the AQMEII initiative focused on evaluating and intercomparing regional and coupled global/regional modelling systems by collaborating with the Task Force on Hemispheric Transport of Air Pollution, Phase 2 (Dentener et al., 2015, HTAP2). Simulation performance followed the strategy adopted in the first two AQMEII Phases, as described in Galmarini et al. (2012, 2015, 2017).

On the other hand, several previous studies had evaluated modelled aerosol optical properties against satellite data from a global view. In Ghan et al. (2001), simulated AOD were within a factor of 2 of AVHRR (Advanced Very High Resolution Radiometer) products and the behaviour of the Ångström Exponent (AE), estimated from POLDER (POLarization and Directionality of the Earth's Reflectances) and SeaWiFS (Sea-Viewing Wide Field-of-View Sensor), was similar to that simulated.

5 Otherwise, both the simulated AOD in Chin et al. (2002) and Reddy et al. (2005) were reproduced with most of the notable features in TOMS (Total Ozone Mapping Spectrometer), AVHRR and MODIS. Moreover, Ginoux et al. (2006) revealed sensitivity to humidity when evaluated against satellite data. Kinne et al. (2003) compared aerosol modules from seven models with MODIS and TOMS, and found large discrepancies over tropical and Southern Hemisphere oceans due to sea salt treatment. Kinne et al. (2006) also discovered a lower simulated AOD among 20 different modules from the AEROCOM Project (0.11

10 to 0.14) than the satellite AOD composite of MODIS, MISR (Operational Microwave Integrated Retrieval System), AVHRR, TOMS, and POLDER retrievals (0.15).

More recent studies are Colarco et al. (2010), who assessed simulated AOD *versus* MODIS and MIRS, and found similar seasonal and regional variability and magnitude over downwinds of the Saharan dust plume, a high bias in sulphate-dominated regions of North America and Europe, and a better agreement over ocean when the sea salt burden was reduced by a factor

15 of 2. Furthermore, Zhang et al. (2012) reported a relative difference in AE of 13.8% with a negative (positive) bias over high latitude regions (oceans), but correlated well for AOD in comparison with MODIS. Finally, Liu et al. (2012) evaluated long-term simulations compared with the satellite composite derived by Kinne et al. (2006) and identified a low bias for AOD, but a good representation of the observed geographical and temporal variations of aerosol optical properties.

Similar studies to ours, which made a seasonal comparison over Europe, are: Jeuken et al. (2001), in which the comparison

20 of AOD calculations with ARST-2 (Along Track Scanning Radiometer 2) on board the European ERS-2 satellite showed an average difference of 0.17-0.19, but a good representation of the observed patterns; Solmon et al. (2006), in which the simulated AOD presented a general underestimation (more pronounced over the Mediterranean Basin), but within the range of AERONET and MIRS over northern Europe, and followed spatial patterns of MODIS and TOMS over both Europe and Africa.

As the above-mentioned aerosol optical properties influence ARI and ACI, a good representation of them is, thus, a key

25 issue to reduce the uncertainty of aerosol effects on the Earth's climate system. Curci et al. (2017) used AQMEII Phase 3 simulations to evaluate the black carbon absorption against AERONET but no works have evaluated against satellite the seasonal representation of optical properties over Europe by the regional models involved in AQMEII Phase 3. For this reason, our main study aim was to evaluate the representation of two main aerosol optical properties, AOD and AE, using the models of the AQMEII Phase 3 initiative over Europe. The evaluation was made by using the remote-sensing observations from the

30 MODIS sensor. Section 2 provides a brief description of the observational and models data, and the evaluation methodology. Section 3 presents the evaluation results. Finally, Section 4 summarises the main conclusions reached.

2 Methodology

In this work, we focused on evaluating aerosol optical properties representation, AOD and AE, over Europe throughout the year 2010. The evaluation was made using remote sensing data from the MODIS sensors on board the Terra and Aqua satellites.

2.1 Model simulations

5 The evaluated simulation data were from the regional chemical-meteorology simulations made over Europe within Phase 3 of the AQMEII framework.

Two different emission data were used. On the one hand, the so-called HTAP_v2.2 (referred to from this point onwards as HTAP emissions). These data were harmonised by the Joint Research Centre's (JRC) Emission Data Base for Global Research (EDGAR) team in collaboration with regional emission experts from different agencies from the United States, Europe and

10 Asia. HTAP emissions covered the years 2008 and 2010, with yearly and monthly time resolutions, and a global geo-coverage with a spatial resolution of $0.1°$. The chemical species were SO_2, NO_x, NMVOC, CH_4, CO, NH_3, PM_{10}, $PM_{2.5}$, BC and OC at the sector-specific level, and there were seven emission sectors (air, ships, energy, industry, transport, residential and agriculture) (Janssens-Maenhout et al., 2015; Galmarini et al., 2017). There were also the so-called MACC emissions (Pouliot et al., 2015), which have been previously used for AQMEII Phase 2 (Galmarini et al., 2015). The data set is a follow-on to

15 the widely used TNO-MACC database (Pouliot et al., 2012), with a base resolution of $\sim 7km$. The provided species were: CH_4, CO, NO_x, SO_x, NMVOC, NH_3, PM_{coarse}, $PM_{2.5}$. A separate PM bulk composition profile file was composed, based on information per source sector per country. The different represented chemical components were EC, OC, SO_4^{-2}, sodium and other mineral components. Fire emissions were included but volcanic and dimethyl sulphide emission (DMS) were not considered (Galmarini et al., 2017).

20 The study period was 2010 and the study domain was Europe. A detailed description of the simulations can be found in Solazzo et al. (2017). However, a brief description of them which focuses on aerosol treatment is provided below, and this information is summarised in Table 1.

The FI1 simulations were made at the Finnish Meteorological Institute (FMI), and the only difference between both FI1 simulations was the type of emissions used (HTAP or MACC). The System for Integrated modeLling of Atmospheric coMpo-

25 sition (SILAM), version 5.4. (Sofiev et al., 2015), was employed with the meteorological input extracted from the European Centre for Medium-Range Weather Forecasts (ECMWF). Sea salt emissions were included, as in Sofiev et al. (2011) (but not from boundaries), as were biogenic volatile organic compounds (VOC) emissions as in Poupkou et al. (2010) and wild-land fire emissions as in Soares et al. (2015). Wind-blown dust was included only from lateral boundary conditions. Gas phase chemistry was simulated with Carbon-Bond Mechanism-IV (CBM-IV), and with updated reaction rates according to IUPAC

30 recommendations (http://iupac.pole-ether.fr) and JPL (http://jpldataeval.jpl.nasa.gov). Secondary inorganic aerosol (SIA) formation was computed with the updated DMAT scheme (Sofiev, 2000) and secondary organic aerosol (SOA) formation with the Volatility Basis Set (Donahue et al., 2006, VBS). AOD in SILAM was computed assuming external mixture of spherical

particles, taking into account their hygroscopic growth. The optical properties used in the Mie computations originate from the OPAC dataset (Hess et al., 1998).

The ES1 simulation was run by the Regional Atmospheric Modelling Group at the University of Murcia (UMU, Spain). They used the Weather Research Forecasting model online coupled with Chemistry (Grell et al., 2005, WRF-Chem), version 3.6.1. Meteorological inputs were driven by ECMWF analysis fields. The aerosol module based on the Modal Aerosol Dynamics Model for Europe (Ackermann et al., 1998, MADE), in which secondary organic aerosols (SOA) were incorporated by the Secondary Organic Aerosol Model (Schell et al., 2001, SORGAM), was used. The employed gas phase chemistry model was the Regional Acid Deposition Model, version 2 (Stockwell et al., 1990, RADM2), with 57 chemical species and 158 gas phase reactions, of which 21 are photolytic. Anthropogenic emissions were MACC emissions. Biogenic VOC emissions were computed by applying the Model of Emissions of Gases and Aerosols from the Nature (MEGAN) emissions model (Guenther, 2006), version 2.04. The MADE/SORGAM sea salt (Gong, 2003) and dust (Shaw et al., 2008) emissions were used.

The IT1 simulation was made at the Ricerca sul Sistema Energetico (RSE, Italy) using the Weather Research Forecasting (WRF) model coupled with the Comprehensive Air Quality Model with Extensions (CAMx), version 6.10. Meteorological inputs were generated using WRF-Chem version 3.4.1. Anthropogenic emission were MACC and biogenic were computed by MEGAN. WRF-Chem was adopted to predict GOCART (Goddard Chemistry Aerosol Radiation and Transport) dust emissions (Ginoux et al., 2001) along with meteorology. Sea salt emissions were computed using published algorithms (de Leeuw et al., 2000; Gong, 2003). The WRF-CAMx pre-processor (ENVIRON, 2014, version 4.2) was used to create the CAMx ready input files by collapsing the 33 vertical layers used by WRF to 14 layers in CAMx, but by maintaining the layers up to 230 m above ground level identical. Aerosol optical properties were estimated by means of the Aerosol Optical DEpth Module (Landi, 2013, AODEM) post-processing tool that was coupled to CAMx regional model. AODEM calculated the optical properties (e.g. AOD, extinction and scattering coefficients, and particle number concentrations) at different wavelengths and size bins starting from the aerosol mass concentration predicted by CAMx. In this work, the Mie theory was applied by dividing the size range (40 nm to 10 μm) into 10 bins, and calculating the hygroscopic growth of each aerosol species in each bin with the Hanel formula. Moreover, particles were assumed to be internally mixed.

The IT2 simulations were run at the University of L'Aquila (Italy) using WRF-Chem (Grell et al., 2005), version 3.6. The modified MADE/VBS aerosol scheme (Tuccella et al., 2015) was included in this version. This scheme is based on MADE to treat inorganic aerosols, along with the VBS approach (Ahmadov et al., 2012). MADE/VBS allows a better representation of the SOA mass. The Regional Atmospheric Chemistry Mechanism - Earth System Research Laboratory (RACM-ESRL) gas phase chemical mechanism (Kim et al., 2009) was used. Anthropogenic emissions were MACC emissions which had been adapted to the chemical mechanism used following the method of Tuccella et al. (2012). As in the IT1 and ES1 simulations, biogenic emissions were calculated online by the MEGAN model (Guenther, 2006). Finally, the meteorological analyses used to initialise WRF were provided by the ECMWF with a horizontal resolution of 0.5° every 6 h. IT2_M-ARI was run with ARI, while large-scale clouds were solved by a simple module. IT2_M-ARI+ACI took into account ARI and ACI, while aqueous chemistry was solved in convective clouds. As well as ES1, IT2 simulations used the MADE/SORGAM sea salt and dust emissions.

Atmospheric
Chemistry
and Physics
Discussions

WRF-Chem simulations, ES1 and IT2, determined aerosol optical properties according to wavelength following Fast et al. (2006), Barnard et al. (2010) and Chapman et al. (2009). The composite aerosol optical properties were determined by the Mie theory, summation over all the size bins and wet particles diameters. An overall refractive index for a given size bin, as determined by an volume averaging of complex indexes of refraction associated with each chemical constituent of the aerosol,

5   was used. The inclusion of ACI and ARI in WRF-Chem is described in Chapman et al. (2009).

Table 1. Model simulations

Model Code	Institution	Meteorological model	Dispersion model	Emissions	Aerosol mechanism	Gas Phase mechanism	Resolution (XY, Z)*
FI1_HTAP	FMI	ECMWF	SILAM v.5.4.	HTAP	DMAT VBS	CBM-IV	0.25°, 12 uneven levels below 13km (1st to $\sim 30m$)
FI1_MACC				MACC			
ES1_MACC	UMU	WRF	WRF-Chem v3.6.1	MACC	MADE-Sorgam	RADM2	23km, 33 levels up to 50hPa (1st to $\sim 21m$)
IT1_MACC	RSE	WRF v.3.4	CAMx v6.10	MACC	Coarse-Fine	CB05	23km, 14 levels up to 8km (1st to $\sim 25m$)
IT2_M-ARI	UAq	WRF	WRF-Chem v3.6	MACC	(ARI) MADE/VBS	RACM-ESRL (Aq. conv. clouds)	23km, 33 levels up to 50hPa 12 below 1km (1st to $\sim 12m$)
IT2_M-ARI+ACI					(ARI+ACI)		

FMI (Finnish Meteorological Institute, Finland), UMU (University of Murcia, Spain), RSE (Ricerca sul Sistema Energetico, Italy), UAq (University of LÁquila, Italy)

*XY: Horizontal resolution; Z: Vertical resolution.

A multimodel ensemble (henceforth referred to as ENSEMBLE) of the available simulations was also evaluated. The results presented herein did not intend to represent an ensemble of opportunity, but were merely calculated as the mean of all the participating simulations. As part of the AQMEII Phase 3 initiative, the available variables of aerosol optical properties were AOD at 470, 550 and 670 nm.

10   ## 2.2 Observational Data

The used observational data came from the twin MODIS (Moderate Resolution Imaging Spectroradiometer) sensors. These instruments, aboard the Terra (MOD04_L2) and Aqua (MYD04_L2) satellites, provide information about aerosol optical properties around the world.

The used data were Level 2 of the Atmospheric Aerosol Product (MxD04_L2) from the collection 6, with a resolution of

15   10 km which are estimated by two different algorithms, Dark Target (DT) and Deep Blue (DB). The used variables were: (1)

Atmospheric
Chemistry
and Physics
Discussions

a "combined" variable of the DT and DB algorithms which provide information about AOD at 550 nm for both ocean and land; and; (2) AE between 550 and 860 nm over the ocean estimated by the DT algorithm. Although this "combined" AOD product has not yet been validated, it offers a wider coverage. The preliminary estimated error (EE) for the used AE products was 0.45 in the pixels with an AOD > 0.2 (Levy et al., 2013). The selection of this observational data was due to results found

5 by Palacios-Peña et al. (2017a).

As Terra and Aqua are in Sun-synchronous orbits around the Earth, MODIS does not provide data over the entire studied domain for each time step. According to Levy et al. (2013), who have established that there is no significant difference between MODIS/AERONET comparability for Terra and Aqua data, we combined the hourly data from both satellites in order to obtain a whole year of data with a wider coverage for each time step than by using the Terra and Aqua data separately.

10 ## 2.3   Evaluation Method

Simulations (Table 1) and satellite data had a different spatial resolution. Henceforth and beforehand, all the data were preprocessed and bilinearly interpolated to a common working grid with a resolution 0.25°.

As mentioned above, our objective was to evaluate the representation of the main aerosol optical properties: AOD and AE. MODIS provides AOD at 550 nm and AE between 550 and 860 nm, but from simulations, the available variables were AODs at

15 different wavelengths. Thus in order to evaluate AE from simulations, this variable had to be estimated through the Ångström empirical expression (Ångström, 1929, eq. 1), where λ is the wavelength and β is Ångström's turbidity coefficient.

$$AOD = \beta \lambda^{-AE} \tag{1}$$

By rationing equation 1 at two different wavelengths and taking algorithms, AE can be computed from the spectral AOD values (Eck et al., 1999, eq. 2). Hence it is possible to estimate AE between two known wavelengths, and to also use this AE

20 to estimate AOD at other different wavelengths. However, as established Ignatov et al. (1998), retrievals of AE under AOD conditions lower than 0.1 are highly uncertain. For this reason, we chose the criteria to estimate AE over areas with AOD > 0.1. Moreover and according to the EE for the AE products of MODIS, we set the AE values range between -0.5 and 4.0.

$$AE = -\frac{ln(\frac{AOD_{\lambda_2}}{AOD_{\lambda_1}})}{ln(\frac{\lambda_2}{\lambda_1})} \tag{2}$$

Once all the data had the same resolution, and following Equation 2, the simulated AOD and AE were at the MODIS

25 wavelengths. Then the hourly data were evaluated using classical statistics such as: the mean of the individual model-prediction error or bias (e_i); i.e., the mean bias error (MBE); the mean of the absolute error (MAE); and the coefficient of determination (r), according to Willmott et al. (1985), Weil et al. (1992) and Willmott and Matsuura (2005). Before the statistical analysis, a mask that showed the areas where the satellite observations were higher than the 10% of their maximum, was implemented. This mask was implemented in order to carry out a statistical analysis with a number of observations which show more confident

30 results. Figures S1 and S2, in the appendix, show the number of observations used when the mask was implemented.

The MBE was estimated as in Equation 3, where i represents each time step, P is the simulation and O is the observational value. MBE provides an idea about the behaviour of the models, and indicates whether the model over- or underestimates the variable values measured by the satellite sensor.

$$MBE = n^{-1} \sum_{i=1}^{n} e_i = \overline{P_i - O_i} \tag{3}$$

5   The MAE was calculated as in Equation 4 and provides an estimation of the magnitude of the error independently of over- or underestimation.

$$MAE = \langle n^{-1} \sum_{i=1}^{n} |e_i| \rangle = \overline{|P_i - O_i|} \tag{4}$$

The temporal determination coefficient was estimated as in Equation 5 and was used as a measure of the strength of the linear relationship between two variables, in our case, the satellite and simulations values.

10     $$r^2 = \langle \frac{n^{-1} \sum_{i=1}^{n}(O_i - \overline{O})(P_i - \overline{P})}{\sigma_O \sigma_P} \rangle^2 \tag{5}$$

Finally, the Kernel probability density functions (PDF) with a broadband of 0.05 were used to evaluate the skills of the simulations to reproduce the variability (temporal and spatial) of the studied variables (AOD and AE).

3   Results

The next section evaluates the skills of the different AQMEII Phase 3 simulations with respect to the representation AOD
15   and AE representation. The first section shows the model evaluation for the AOD representation and the second for AE. The numerical result of each case is indicated by the numbers represented in each figure. Finally, the skills of the simulations to reproduce the variability of the studied variables (AOD and AE) are analysed using the PDF of each variable.

3.1   Model evaluation of the AOD representation

AOD is defined as the integrated extinction coefficient over a vertical atmospheric column and indicates to what degree aerosols
20   avoid light transmission. AOD is not a direct function of the atmospheric load of particles, but can provide us an approximate idea of both atmospheric load of particles and the interaction of these particles with radiation.

First, temporal means of AOD at 550 nm values from a combination of the two MODIS satellites were analysed in the first row of Figures 1, 2 and 3. The temporal mean for the whole year is show in figures in the supplementary material (SM). The seasonal break down is presented besides named. JFM represents the temporal mean for January, February and March (from
25   now on winter); AMJ for April, May and June (spring); JAS for June, August and September (summer); and finally, OND for October, November and December (autumn).
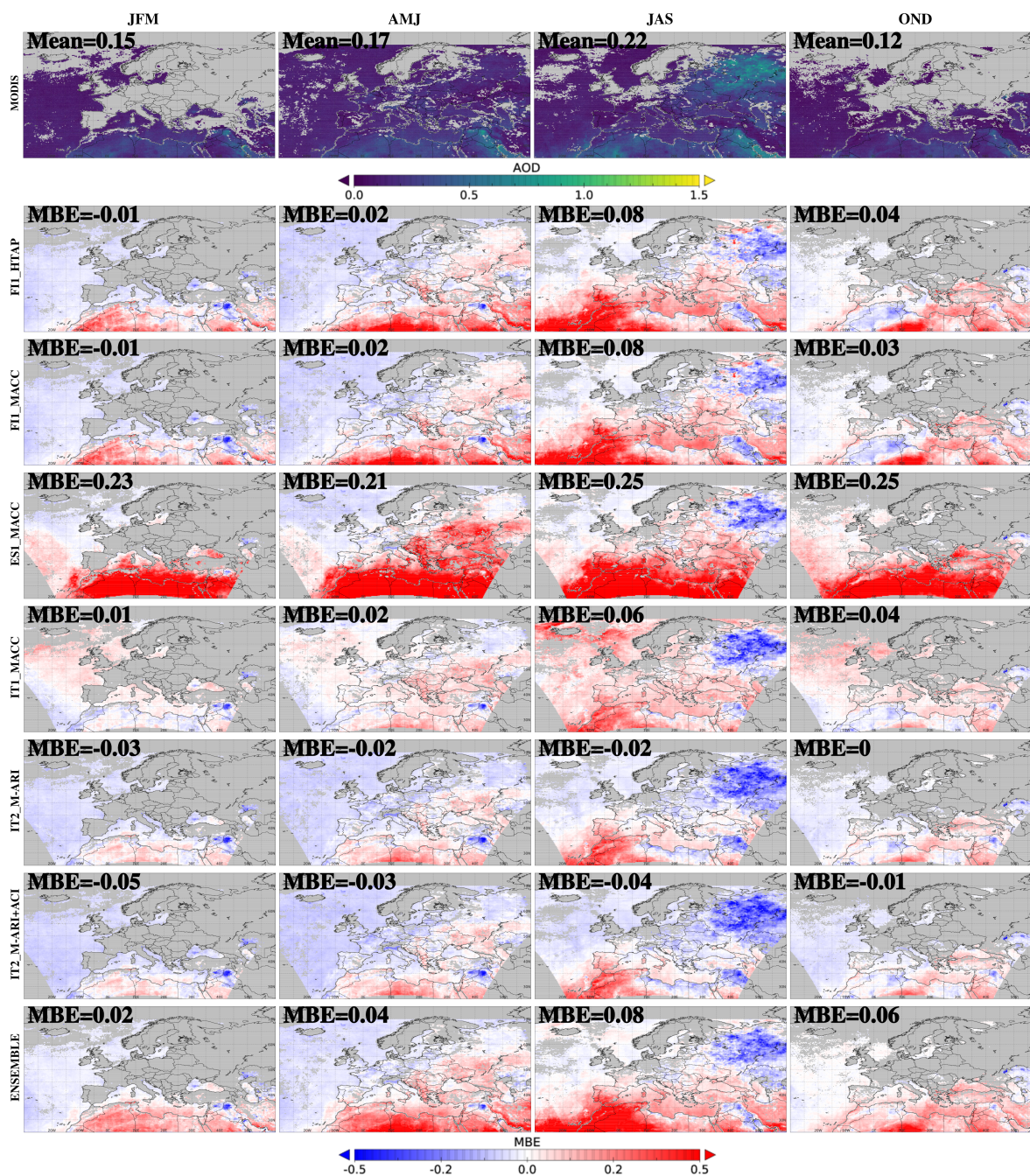
Figure 1. The MBE results of AOD at 550nm satellite values *vs.* simulations. Columns from left to right, temporal mean of: winter (JFM), spring (AMJ), summer (JAS) and autumn (OND). First row: satellite values; and from second row to the bottom, the MBE values of: FI1_HTAP, FI1_MACC, ES1_MACC, IT1_MACC, IT2_M-ARI, IT2_M-ARI+ACI and ENSEMBLE

The temporal mean of AOD (Figure S3 at SM) for the whole year 2010 presented the highest values (between 0.5 and 1) over Russia and the surrounding areas, and over the south of the domain and the Mediterranean Region.

When seasonal figures were analysed (Figure 1), the highest values (around 1) were found over the southern part of the domain for all seasons due to frequent Saharan desert dust outbreaks, which affects the Mediterranean Region. Moreover,

5   these desert dust outbreaks were more frequent and strong for spring and summer because the mean AOD values were higher.

In spring, the highest temporal mean AOD values, between 0.5 and 1, reached the southern part of the domain. These mean values can be higher than 1 over specific areas.

In summer, the temporal mean AOD values over the southern part of the domain fell between 0.5 and 0.8, but the higher mean AOD values (above 1.5) were found over a large area in Russia and its surrounding areas. During this period, a heat wave

10   and wildfires occurred over this area, which explained this fact. For these two reasons, this season presented the highest mean AOD values when both space and time were considered.

However for autumn and winter, high mean AOD values were also found over the southern part of the domain, but were lower than 0.5. The lower mean AOD value when considering space and time was found in autumn. It is noteworthy that ice, snow and clouds were avoided for the MODIS sensor, and aerosol properties were not retrieved over the areas where they were

15   present (http://darktarget.gsfc.nasa.gov/), which explains the gap over the northern part of the terrestrial domain in winter and autumn. The gaps in the rest of the season are explained by the implemented mask, which is explained in the Observational Data Section.

Throughout the seasons, high AOD values were obtained over the south-eastern part of the domain; Syria, Iraq, Kuwait and the Persian Gulf.

20   According to MBE, all the simulations spatially presented a similar behaviour throughout the year (SM) and in different seasons (Figure 1). The main feature was an overestimation of AOD over the southern part of the domain, the main area affected by desert dust outbreaks; and an underestimation (to a greater or lesser extent) over the Russian area, affected by the wildfire emissions in summer.

Throughout the year, FI1_HTAP and FI1_MACC, which use the ECMWF model for meteorology and SILAM for chemistry,

25   showed a slight overestimation of the AOD values. These values were overestimated over the southern part of the domain (northern part of the Saharan Desert), with values around 0.1. These values were spatially consistent with the higher MAE values (see second column of Figure S3 at SM). Over north-western areas and Russia (due to the wildfires that occurred in summer), these simulations underestimated AOD (negative MBE values around -0.05). One main issue is that no clear differences were found when HTAP and MACC emissions were used.

30   The other simulations; ES1_MACC, IT1_MACC, IT2_M-ARI and IT2_M-ARI+ACI; used the WRF meteorological model. When a different chemistry model was employed, minor differences in the error of simulations were found between those made using the CAMx chemistry model (IT1_MACC) and the WRF-Chem (IT2 simulations). These differences were of a similar order of magnitude to that of the differences between the IT2 simulations by including ARI and ACI. However, the ES1_MACC simulation which, like the IT2 simulations, used WRF-Chem, presented remarkable differences by displaying a

35   strong overestimation of AOD over the southern areas of the domain. Thus ES1_MACC showed the higher MBE and MAE
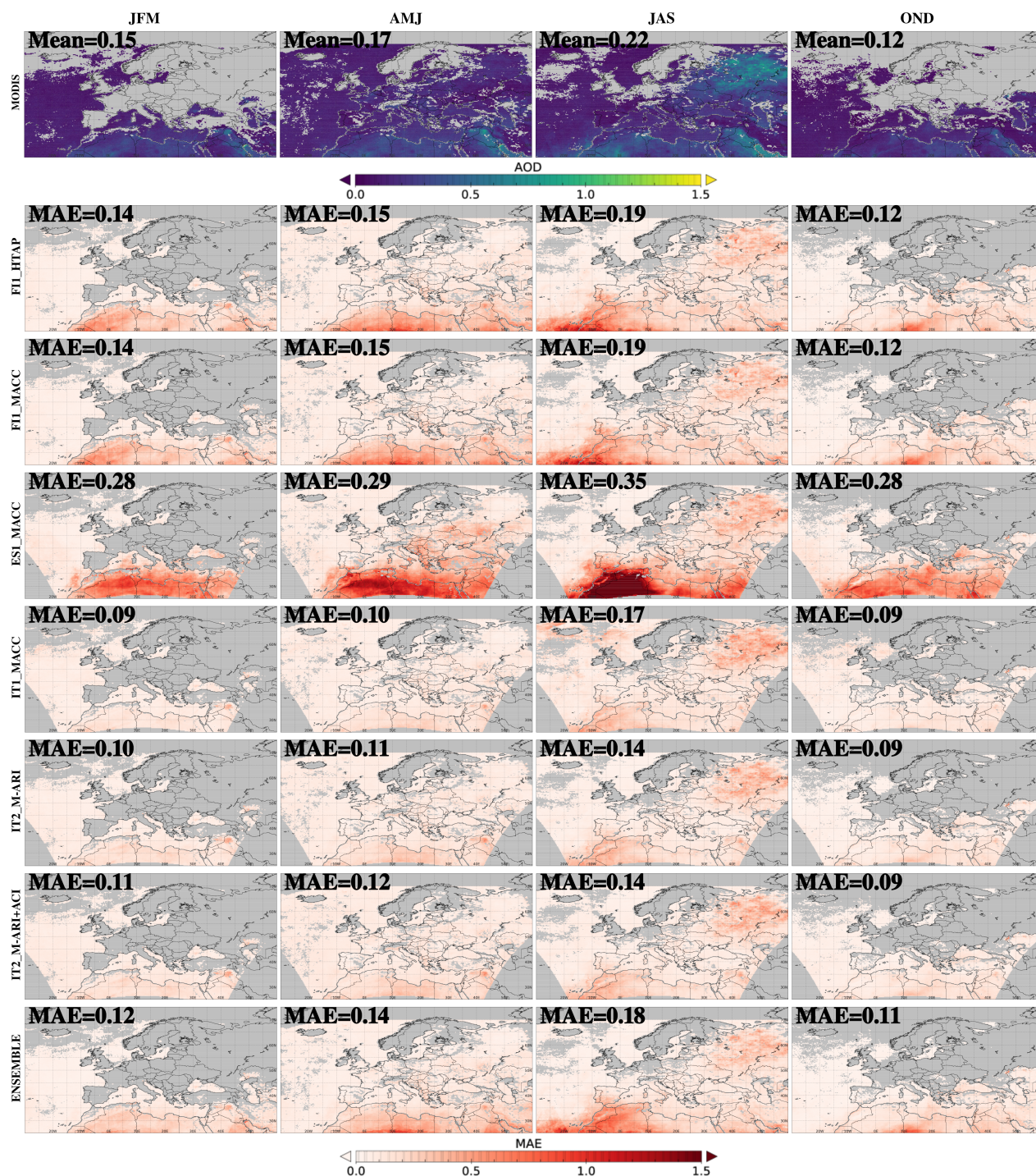
11

Figure 2. Idem Figure 1 for the MAE results of AOD at 550nm satellite values *vs.* simulations.

values throughout the year. Despite this overestimation, a slight underestimation was seen over Russian areas (negative MBE values around -0.05).

IT1_MACC presented a general weak overestimation of AOD over the whole domain. This simulation over Russia underestimated the AOD values (negative MBE values around -0.1), which was due mainly to the wildfires that occurred in summer.

5 The IT2 simulations displayed a different behaviour. These simulations presented a general weak underestimation over the whole domain (MBE of -0.03 and -0.05 for ARI and ARI+ACI, respectively), except over the southern part of the domain (areas affected by the Saharan dust outbreaks), where AOD was overestimated with low values. The underestimation of AOD was stronger over the northern part of the domain (particularly over Russian areas) and reached mean values of around -0.2. The IT1_MACC and the IT2 simulations presented the lowest absolute error values.

10 The ENSEMBLE notably overestimated the AOD values over the southern part of the domain, with very high values over the northern part of the Saharan Desert, which is consistent with the higher MAE values obtained for the whole year of ENSEMBLE. The underestimation was milder than the overestimation, and pointed it out over the Russian areas affected by wildfires.

One notable point in the underestimation was presented by all the simulations over the south-eastern part of the domain
15 (represented as a blue spot), centred over Iraq. The ES1_MACC simulation did not show this underestimation because of its high AOD values, but presented lower overestimation values (close to 0) over this area than over its surroundings. This small spot was also notable when MAE (Figure 2) was analysed.

In winter (the first column in Figures 1 and 2), all the simulations presented a weak underestimation over the Atlantic Ocean, except for IT1_MACC, which presented a weak overestimation in the northern part (MBE mean of 0.03). The above-mentioned
20 blue spot was clearly defined over a small south-easterly area and was stronger during this season, even for the ES1_MACC simulation with negative MBE values. For the IT1_MACC, IT2_M-ARI and IT2_M-ARI+ACI simulations, the higher MAE values were consistent over the last mentioned area. The FI1 simulations presented an overestimation over North Africa. This area was larger with a stronger overestimation (mean MBE of 0.23) for the ES1_MACC simulations for the same reason explained above. All year long, these simulations showed higher MAE values (a mean of 0.28). The ENSEMBLE presented an
25 intermediate behaviour, with milder MBE and MAE values (0.02 and 0.12, respectively): an overestimation of the AOD values over North Africa, a very weak underestimation over the Atlantic Ocean and the blue spot centred over Iraq and Syria.

In spring (the second column in Figures 1 and 2), the underestimation of AOD was similar to that in winter, but with steeper values. All the simulations presented an overestimation (with different degrees) over the southern part of the domain, the Balkan Peninsula and southern Russia. This overestimation was larger and stronger for the ES1_MACC simulation (MBE of 0.21) and
30 once again presented higher MAE values (0.29). All the simulations, except for IT1_MACC, presented a weak underestimation over the Atlantic Ocean. The IT simulations gave fewer errors than the rest. As in winter, a small south-easterly area (the blue spot) appeared, but was consistent with the maximum MAE values for the IT simulations.

The underestimation of AOD due to the wildfire emissions over Russia and the surrounding areas was one of the most important issues in summer (the third column in Figures 1 and 2). This underestimation was larger and stronger for the IT2
35 simulations, and was smaller and weaker for the FI1 simulations. Moreover, the aforementioned small area in the south-eastern
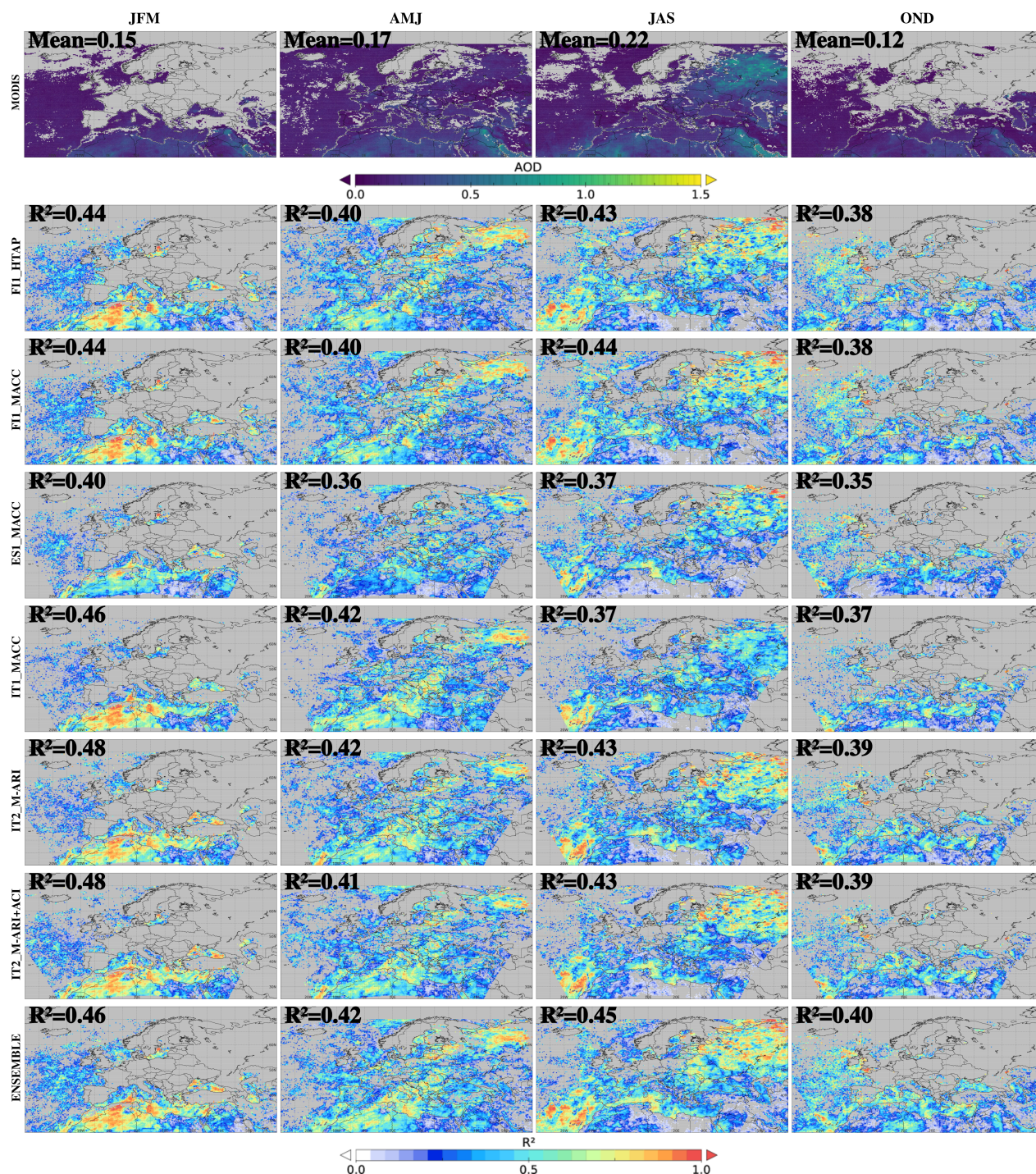
Figure 3. Idem Figure 1 for the determination coefficient of AOD at 550nm satellite values *vs.* simulations.

part of the domain presented higher underestimation values over a larger area than during the other seasons, and reached as far as the Persian Gulf. The overestimation behaviour was the reverse of the underestimation; the FI1 simulations presented higher values and the IT2 ones gave lower values. While the overestimation was stronger and affected a large area than during another season, this time the higher overestimation values were found over the north-west areas of Africa and the Iberian Peninsula.

5   As during the other seasons, the ES1_MACC simulation showed the stronger and larger overestimation. During this season, with higher AOD values, all the simulations presented the highest error values. The ENSEMBLE represented the most relevant behaviour of MBE and MAE, which means that the important evaluation results were found over those areas where other simulations presented a notable issue (mainly the south-western part of the domain, Russia and the surrounding areas, and the "blue spot").

10   In autumn most of the domain presented error values that came close to 0 for all the simulations. Thus autumn was the season when the lowest error values were found. All the simulations showed an overestimation that came close to the south boundary and an underestimation over Tunisia and Algeria. Both the overestimation and underestimation were weaker for the IT simulations than for the FI1 ones. ES1_MACC was the only simulation that displayed a different behaviour during this season with a high overestimation over almost all the domain (0.25).

15   Regarding the coefficient of determination, only the areas where the results were significant at 90% are shown. All the simulations presented values above 0.5 over most of the domain. Throughout 2010 (Figure S3 at SM) the values of this statistics were lower than when the seasonal breakdown was analysed (Figure 3). ENSEMBLE presented the highest values and over a largest area (in detail over Russian and the surrounding areas, and over the south-western part of the domain), while the ES1_MACC simulation presented the smallest area and, thus, the lowest mean value.

20   In winter the highest determination values (close to 1.0) were found over the north-eastern part of the African continent. In spring, these high values were found over central and eastern parts of Europe and North Africa. In summer, the highest values were mainly over Russian and the surrounding areas and a part of the Atlantic Ocean in the south-western part of the domain. Finally in autumn, the coefficient of determination values were lower than for the other seasons, and were mainly over the Mediterranean sea and the Atlantic Ocean.

25   ## 3.2   Model evaluation of the AE representation

AE is a parameter that indicates the relationship between the size of the particles suspended in the atmosphere and the wavelength of the incident light, and, although there is not a direct correspondence between aerosol size and AE, provides an idea of the size of particles. Low AE values are related to coarse particles, such as desert dust or sea salt, and high values are associated with fine particles, such as anthropogenic source particles or biomass burning. The AE values are between 0 (or even slightly

30   negative in coarse mode aerosol episodes) and 4 (Boucher, 2015).

Temporal mean of AE between 550 and 860 nm satellite values, which are only estimated over the sea, is showed in the first row in the AE figures (Figures 4, 5 and 6 and S4 at SM).

Throughout the whole year (Figure S4 at SM), low AE values (below 0.5) were found offshore, where sea salt particles (coarse) predominated. Over the Mediterranean coast near the Saharan desert, low values were found due to the frequency of
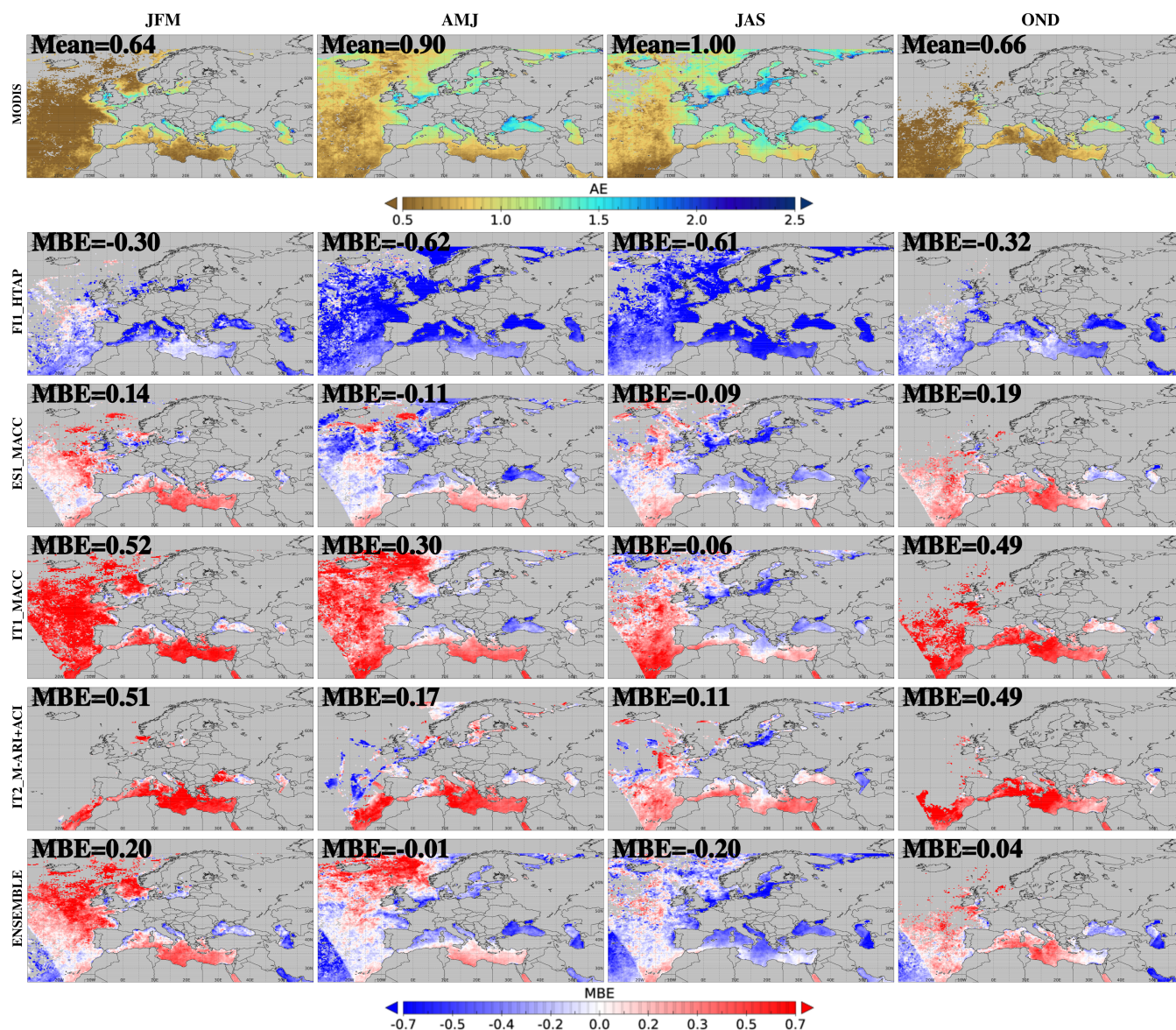
Figure 4. MBE results of AE between 550 and 860nm satellite values *vs.* simulations. Columns from left to right, temporal mean of: winter (JFM), spring (AMJ), summer (JAS) and autumn (OND). First row: satellite values; and from the second row to the bottom, the MBE values of: FI1_HTAP, ES1_MACC, IT1_MACC, IT2_M-ARI+ACI and ENSEMBLE.

desert dust outbreaks. High values (between 1.5 and 2.0) were obtained over coasts in central Europe. These values were due mainly to anthropogenic emissions, such as traffic road, which presents fine particles. Moreover, these values lowered from the coast to offshore. This pattern also showed when seasons were separately evaluated. Two small areas over the north of the Black and Caspian sea, showed values around 2.5.
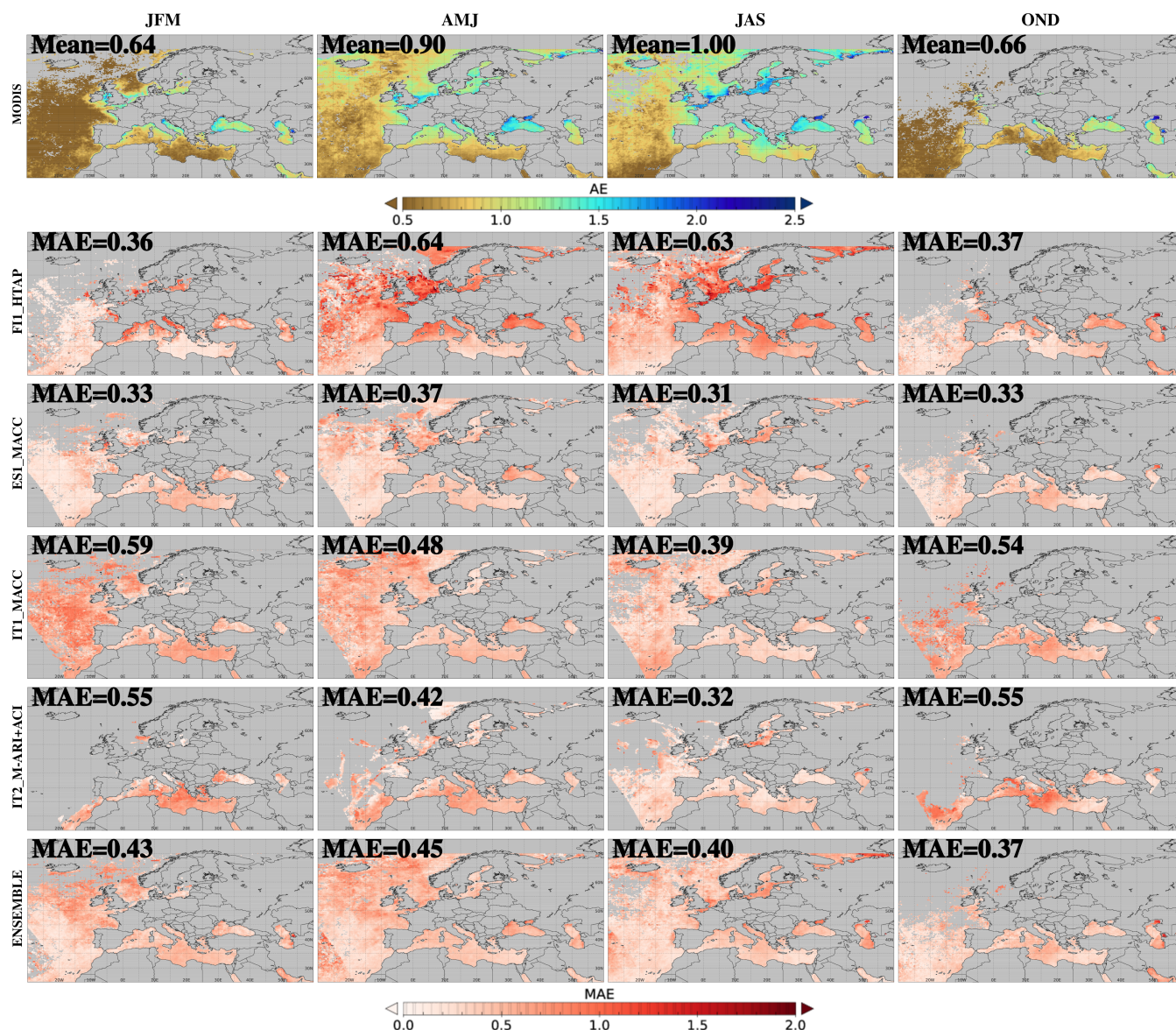
Figure 5. Idem Figure 4 for the MAE results of AE between 550 and 860nm satellite values *vs.* simulations.

In winter (JFM, the first column in the first row in the AE figures) and autumn (OND, fourth column), the lowest values were found over the Atlantic Ocean and the Mediterranean Sea. In the same way as throughout the year, high AE values (around 1.5) were shown over coasts in central Europe. In autumn, a small area over the north of the Caspian sea with values of 2.5 was found.

5   In spring, as represented in the second column (AMJ) in the first row in the AE figures, the AE values presented a narrow range between 1.0 and 1.5 over most of the domain. Some exceptions were values that came close to 0.5 near the African

Atmospheric
Chemistry
and Physics
Discussions

continent, and values close to 2.0 over coasts in central and north Europe. It is noteworthy that low AE values (close to 0.5) were uniformly distributed in spring over the southern part of the domain, while in summer (JAS, the third column in the first row in the AE figures) the lowest AE values (lower than 0.5) were found mainly over the southern Atlantic Ocean. Values between 2.0 and 2.5 were estimated over north-eastern coasts and the north of the Black and Caspian sea, which were lower

5   than in summer.

In this section, the simulations run with the available data were less than they were for AOD. The errors of the simulations made for the whole year are shown in Figure S4 at SM.

Throughout the year, FI1_HTAP (the ECMWF meteorological model and the SILAM chemistry model) underestimated the AE over most of the domain (MBE of -0.60). This underestimation was higher over areas near European coasts, where the

10   satellite showed values of around 1.5, which were lower over the south-western part of the domain, where the satellite gave AE values that came close to 0.5. This simulation also presented the highest MAE values.

In spite of the results obtained for the AOD representation evaluation, ES1_MACC is the simulation which presented the lowest error values (MBE and MAE) over the whole year. A very low overestimation was found over areas close to Africa, and a more notable underestimation was found over areas near the European coast (MBE of -0.1).

15   The IT1_MACC simulation generally overestimated the AE values over the Atlantic Ocean and the Mediterranean Sea (the areas with AE values that came close to 0.5). Over the areas near the coast of central and northern Europe, where the satellite gave values around 1.5, this simulation presented a weaker underestimation than in the other simulations.

The IT2_M-ARI+ACI simulation showed an overestimation over the Atlantic and Mediterranean coast near North Africa (MBE of 0.14), and a weak underestimation over the coasts of the North and Baltic Seas. This simulation along with ES1_MACC,

20   which used the WRF-Chem model, gave the lowest values of MAE.

Finally, ENSEMBLE presented a notable underestimation of the AE values over the European Coast (including the Mediterranean Sea), probably due to the strong underestimation provided by the FI1_HTAP simulation. Very low overestimation values were obtained over the Atlantic Ocean and near African coasts in the south Mediterranean Sea. Moreover, ENSEMBLE and the other simulations presented a strong underestimation over the two small areas with AE values of around 2.5.

25   In order to gain better knowledge of model skills, a seasonal study was conducted. Winter is represented in the first column in Figures 4 and 5. The FI1_HTAP simulation generally showed an underestimation of the AE values, which was stronger over areas near the European coast. The ES1_MACC simulations presented the lowest error values. This simulation displayed a weak overestimation of the AE values over the Atlantic Ocean and the Mediterranean Sea, and an underestimation over small areas close to the European coast. Both the IT1_MACC and IT2_M-ARI+ACI simulations gave a general overestimation over

30   most of the domain. IT1_MACC showed a very weak underestimation close to the European coast, but this simulation had the highest MAE values due to the strong overestimation. ENSEMBLE gave high overestimation values over the North Atlantic and the Mediterranean Sea, and weak underestimation values close to the European coast.

The second column of Figures 4 and 5 shows the results obtained in spring. For this season, FI1_HTAP underestimated the AE values over most of the domain and presented the highest error values (MBE of -0.62 and MAE of 0.64). The ES1_MACC

35   simulation displayed a behaviour somewhere between the other simulations, with a weak overestimation over the North Africa
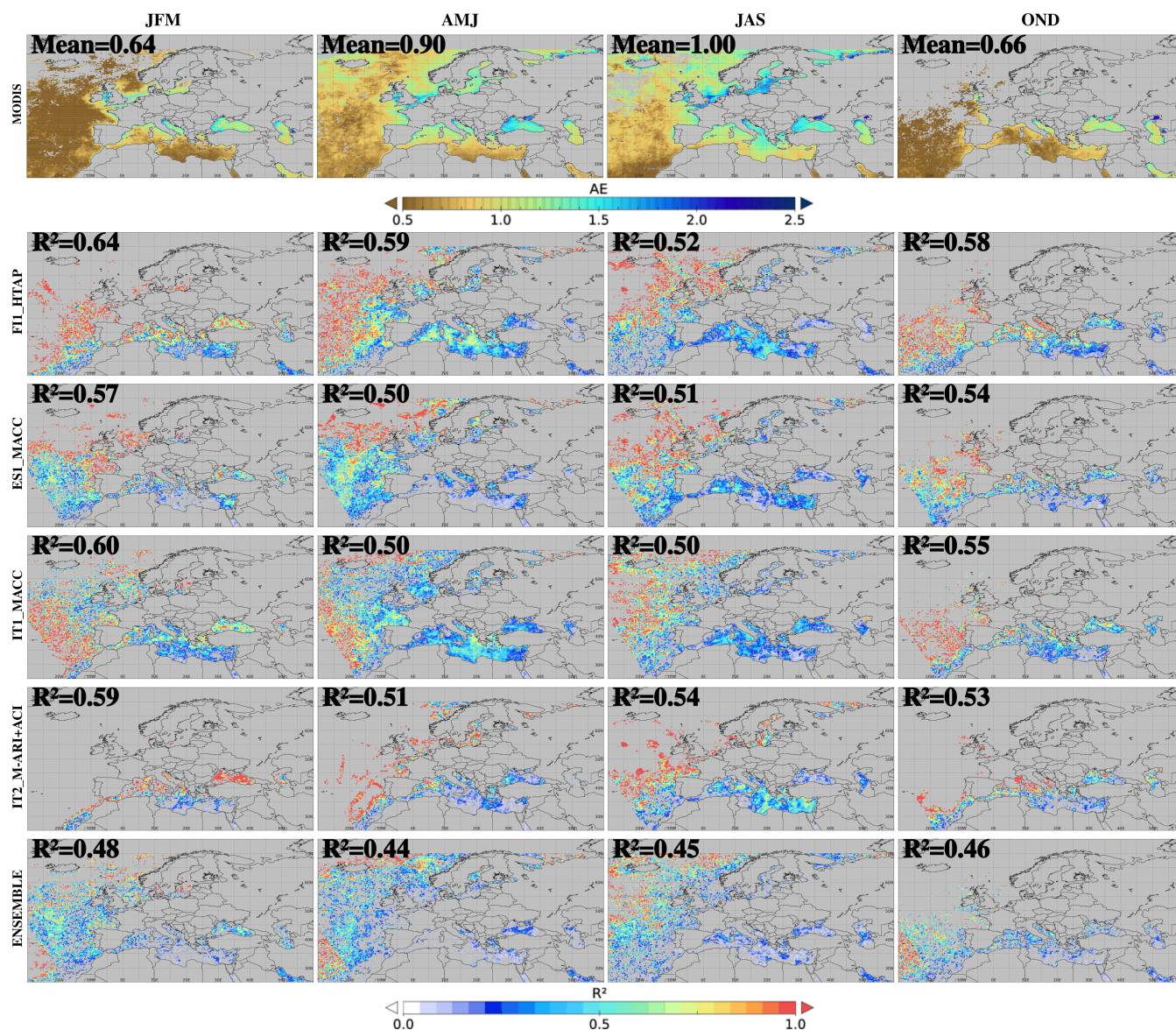
Figure 6. Idem Figure 4 for the determination coefficient of AE between 550 and 860nm satellite values *vs.* simulations.

coast and a more notable underestimation over the northern part of the domain. Notwithstanding, the ES1_MACC simulations presented the lowest absolute error values. The IT1_MACC simulation overestimated the AE values over the Atlantic Ocean and the southern part of the domain, and the underestimation was found in areas over the European coast. The IT2_M-ARI+ACI simulation overestimated the AE values over the Moroccan Atlantic coast and the Mediterranean Sea, but small areas of

5 underestimation were found over the Azores Islands and the northern coast of France. Finally, ENSEMBLE produced a general

underestimation over most of the domain. The overestimation was produced mainly over an area that lies north of the British Isles, where satellite values came close to 0.5.

All the simulations made in summer (the third column in Figures 4 and 5) displayed similar skills as in spring. Generally speaking, FI1_HTAP underestimated the AE values and presented the greatest errors. During this season, ES1_MACC showed

5 a larger area of underestimation and a smaller one of overestimation, but with similar error values as in spring. The overestimation of the IT1_MACC simulations was weaker, but the underestimation was stronger and over a large area over the North and Baltic Seas. The IT2_M-ARI+ACI simulation also produced an overestimation over most of the domain, but it was weaker than that presented in spring. Notwithstanding, this simulation presented a small area of underestimation over the Baltic sea. However, ENSEMBLE displayed a general underestimation that lowered from the coast to offshore.

10 In autumn (the fourth column in Figures 4 and 5), the behaviour of simulations was similar to that shown in winter. FI1_HTAP produced a general, but weaker underestimation than in spring and summer. During this season, ES1_MACC produced a general overestimation, but once again it gave the lower error values. The IT1_MACC and IT2_M-ARI+ACI simulations overestimated AE values over most of the domain with similar MBE and MAE values. Finally, ENSEMBLE produced a weak overestimation over the Atlantic Ocean and the Mediterranean Sea, and a weak underestimation over the Black, Caspian

15 and Red seas. ENSEMBLE was the simulation with the lowest MAE error.

Figure 6 shows the results of the determination coefficient, which were significant at 90%. These results were worse throughout the year (column third in Figure S4 at SM) than when the different seasons were evaluated. FI1_HTAP and IT1_MACC showed relatively high values (around 0.5) over the Mediterranean Sea, but over this area, all the other simulations presented values above 0.25. Even though the determination values were higher during the seasonal study, it was very difficult to find a

20 clear coefficient of determination pattern. During each season FI1_HTAP was used to present the highest determination values and ENSEMBLE the lowest ones.

3.3 Variability

A good approach to evaluate the spatial and temporal variability of a variable is the Probability Density Function (PDF). This represents the density of counts for each value of the variable. In order to study how the AQMEII Phase 3 simulations

25 represented the variability of AOD and AE, the PDF of both variables for each studied season are shown in Figure 7. In that Figure, left column corresponds to the AOD and right to the AE PDF; first row corresponds to winter (JFM), second to spring (AMJ), third to summer (JAS), and bottom row to autumn (OND). Observed satellite values was represented by a black line; the ENSEMBLE by a red line; FI1 simulations by green dashed lines; ES1 by a yellow dashed line; IT1 by a cyan dashed line; IT2_M-ARI by a blue dashes line and finally IT2_M-ARI+ACI by a blue dotted line.

30 The PDFs of AOD for the data that corresponded to winter (JFM), spring (AMJ) and autumn (OND) presented a similar behaviour. The observed satellite values showed a high probability for low values (between 0 and 0.5). The PDF of the IT1_MACC values for these seasons was the most similar one to the observed MODIS values. For these three seasons, this was the simulation with a lower absolute error when the temporal standard deviation from the simulations was evaluated against observations, as we can see in the SM.
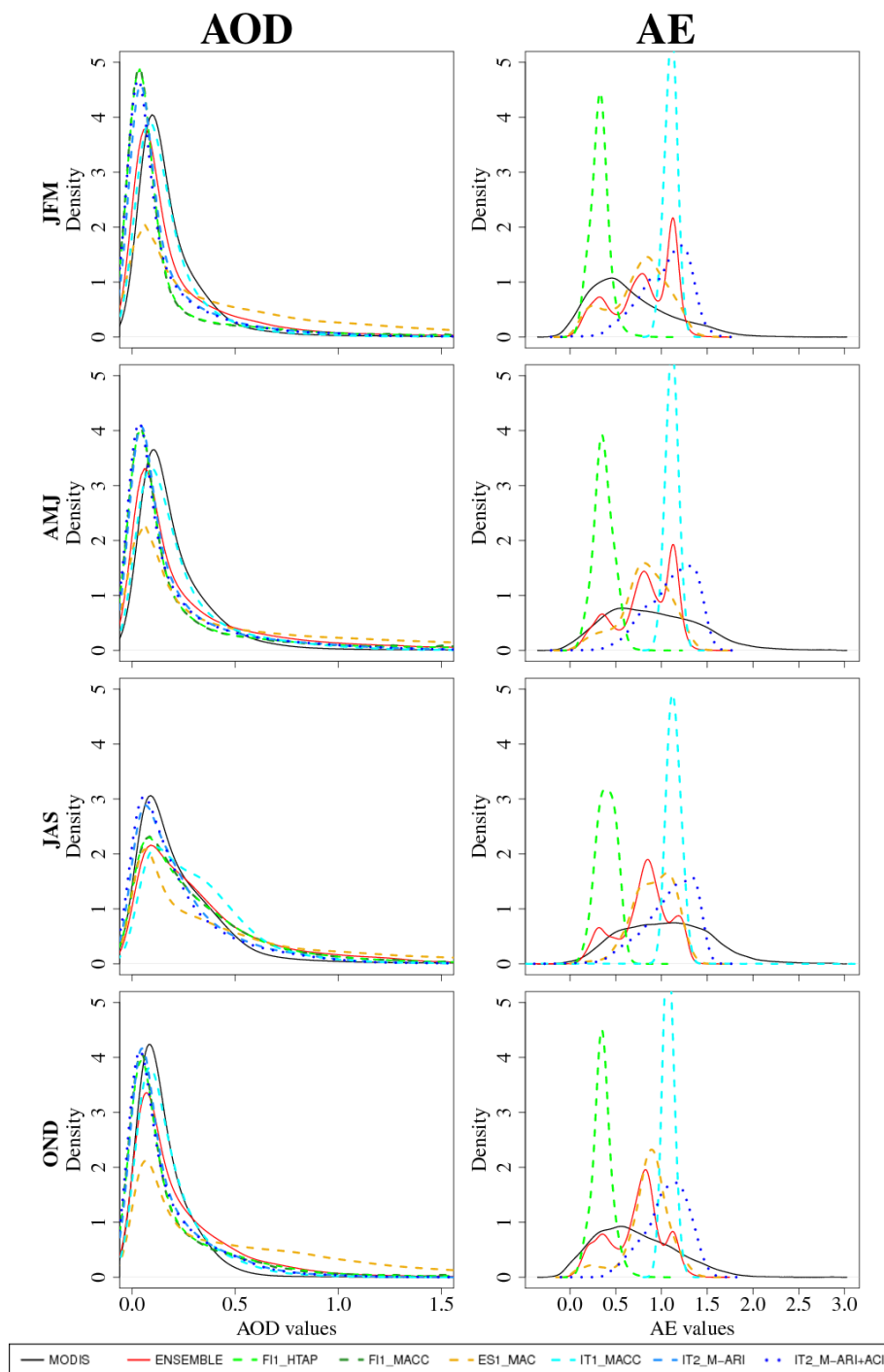
Figure 7. PDF for AOD (left column) and AE (right) values. From the top to the bottom: JFM, AMJ, JAS, OND.

Simulations FI1 and IT2 displayed analogous PDFs with the highest probability for the lower AOD simulated values than those observed. In winter (JFM) and autumn (OND), the IT2 simulations presented higher probabilities for the lower AOD values than the FI1 simulations. However in spring (AMJ), these four simulations gave almost equal PDFs.

The ES1 simulation showed a remarkable representation of AOD in all seasons. The PDFs for this simulation estimated

5   higher probabilities for the high AOD values than the other simulations and the observed values. For this reason, the probability of low AOD values was lower than for the rest. ENSEMBLE displayed in JFM, AMJ and OND a high probability for the lower AOD simulated values than those observed, but with ENSEMBLE, the probability for the higher AOD values was higher than for those observed.

The PDFs of the AOD representation were different in summer (JAS). For this season, both IT2 were the simulations

10   that displayed the nearest behaviour to the observed PDF values. As seen in the SM, these simulations displayed the lowest MAE compared with the observed standard deviation. All the simulations and ENSEMBLE in this season presented a higher probability for the high AOD values than those observed.

The second column of Figure 7 represents the PDFs for the AE values. As for AOD, winter and autumn presented similar PDFs. The observed AE values showed a high probability for the low AE values, around 0.5, and a low probability for the

15   high AE values. For spring and summer, the PDFs for the observed values were tray-shaped, with a high probability for the AE values between 0.5 and 1.5.

The behaviour of the other simulations and ENSEMBLE was similar in all seasons. The FI1_HTAP simulation displayed a high probability for very low AE values, between 0 and 0.6. IT1_MACC gave similar PDFs for all the seasons, and a high probability was found for the AE values between 1 and 1.5. FI1_HTAP and IT1_MACC were the simulations with the

20   narrowest PDFs, which indicates that these simulations produced a strong underestimation of the observed variability of AE (as also indicated in the evaluation of the temporal standard deviation shown in the SM).

The PDFs for ES1_MACC, IT2_M-ARI+ACI and ENSEMBLE were wider than for the other two simulations. ES1_MACC showed a high probability for the AE values, between 0 and 1.5. IT2_M-ARI+ACI for the AE values was between 0.5 and 1.5. ENSEMBLE showed a high probability that ranged from 0 to 1.5. Notwithstanding, these PDFs were narrower than the PDF

25   for the observed values, thus all the simulations underestimated the representation of the AE values. This is observed in the SM, where the estimation of the MBE of the standard deviation gave negative results for all the seasons and simulations.

4   Summary and Conclusions

Although AQMEII Phase 3 focuses on evaluating and intercomparing regional and linked global/regional modelling systems, an evaluation of the simulations of the front observations was needed. Solazzo et al. (2017) analysed the performance of

30   models for different meteorological variables and chemical species. In order to perform a more detailed analysis of the models' performance, this work focused on evaluating the aerosol optical properties representation by means of AQMEII Phase 3 simulations using satellite sensors. The evaluation of these variables is important because they strongly influence ARI and ACI and, thus, influence the atmospheric aerosol effect on the climate system.

As the Mediterranean Region is frequently affected by Saharan desert dust outbreaks, and an area over Russia and the surrounding during summer affected by wildfires, presented the highest AOD values for 2010. When the representation of this variable was evaluated from the MODIS observation, generally all the simulations presented similar spatial patterns and gave a good representation of the low and medium AOD values. The lowest AOD underestimations for all the simulations were found

5   over the Atlantic Ocean and, thus, sea salt emissions could be underestimated. However, a major underestimation occurred during the wildfires episode over Russia in summer. As established in Palacios-Peña et al. (2017a), this underestimation may be due to a misunderstanding of the simulation of the aerosol vertical and may, therefore, be due to the AOD representation given the understated injection height of the total biomass burning emissions found for the MACC emissions by Soares et al. (2015). A different hypothesis ascribes this underestimation to underestimated emissions. Toll et al. (2015b) found that while

10 the daytime plumes from large fires were indeed lifted higher, the night time emissions and emissions from small fires were injected closer to the ground, making the average smoke transport distance even smaller than for the fixed emission height. Also Soares et al. (2015) point out, referring to Wooster et al. (2005), that MODIS is not sensitive enough to register the fire radiative power of small or smoldering fires, and thus large fraction of those is missed in the emission data, including also strongly emitting peat fires. The 2010 Russian fires included some huge fires, but also numerous small ones over large areas,

15 and a large fraction of those was probably missed by MODIS.

Moreover a high underestimation was produced for all the simulations, irrespectively of the used meteorological and chemical model, over a small area in the south-eastern part of the domain (the above-called "blue spot"). This can be explained by the fact that the emissions inventories used herein only covered European areas (see the Emission Map in the SM), thus the emissions over that area were not considered.

20 The AOD over the southern part of the domain was overestimated and related mainly to the high dust concentrations according to the boundary conditions. In line with this, Solazzo et al. (2017) found that the error in primary species as dust was strongly affected by the emission and boundary conditions in the AQMEII Phase 3 simulations.

On the whole, the FI1 simulations, which used the ECMWF files as SILAM model input, gave high AOD values because SILAM is known to have slower dry particle deposition than other models. This could explain that, although the band quiet

25 crudely represents size distribution, AOD is also very sensitive. IT1, which used the WRF meteorological conditions as CAMx model input, displayed quite a reasonable AOD representation skill. ES1, which used WRF-Chem, presented a high AOD overestimation due to the dust outbreaks. This marked overestimation took place because of a bug in the used dust scheme, which lacks the gravitational settling. Although the IT2 simulations used the same dust scheme and model version, the dust flux was modified for these simulations to estimate accurate dust concentrations. The IT2 simulations presented similar patterns to

30 simulations FI1 and IT1, but obtained lower AOD values. No important differences were observed for the AOD representation among the IT2 simulations when the ARI and ACI and aqueous chemistry in convective clouds were solved (IT2_M-ARI+ACI) *versus* the ARI and large-scale clouds only being solved by a simple module (IT2_M-ARI).

It is important to highlight that for all the simulations and seasons, the highest determination values were obtained over the areas with medium AOD values (observed values between 0.5 and 1.0), which were approximately the areas with the lowest

error values. Thus the temporal representation of the medium AOD values by all the simulations was acceptable. The use of an ensemble as the means for all the participant simulations improved this statistical figure.

The AE satellite values were obtained only over sea. High AE values, which indicate fine particles, were found near central European coasts which were higher in summer, probably due to the wildfires that occurred then. Low AE values, which indicate

5 coarse particles, were observed over the southern part of the domain, close to the Saharan desert and over the Atlantic Ocean. It was also noteworthy that the AE values over the Atlantic Ocean were generally much higher in spring and summer than in autumn and winter. This means that the aerosol particles over ocean areas and near the coast in warm months were apparently finer than in colder months. This might be related to two different hypotheses: weaker winds in warm months or hygroscopic growth, which could be greater in cold months generally because of higher relative humidity (RH).

10 AE modelling skills were lower than for AOD (larger errors). The simulation run with the SILAM model and driven by ECMWF meteorological inputs (FI1_HTAP) largely underestimated AE over most of the domain. Hence, this model estimated larger-sized particles than that retrieved by satellite observations. As aforementioned, SILAM crudely represents size distribution, which impacted the AE representation because it may have be centered on particles with a larger diameter. The simulations using WRF coupled CAMx model (IT_MACC) and both WRF-Chem simulations (ES1_MACC and IT2_M-ARI+ACI) under-

15 estimated high AE values and overestimated low AE values. Thus, they underpredicted the variability of this variable. These results are similar to those established in Palacios-Peña et al. (2017b, a). On the other hand, Solazzo et al. (2012); Balzarini (2013); Solazzo et al. (2014) found a severely underestimate for PM_{10} concentrations over Europe for WRF-CAMx and WRF-Chem models, which could explain the overestimation of low AE values. These authors also found an underestimation of $PM_{2.5}$ concentrations which could also explain the underestimation of high AE values since simulated particles underestimate

20 the variability of the size. An interesting fact is shown for ES1_MACC. Despite the lack of dust gravitational settling, it presented the lowest error values for AE. This could be explained by the high dust concentration over southern areas, resulting in low AE values and thus compensating the tendency for producing high $PM_{2.5}/PM_{10}$ ratios.

It was not possible to find any clear spatial pattern for the coefficient of determination of the AE representation. One striking fact in this case was that using the mean of all the simulations as ENSEMBLE did not improve this statistical figure. In fact the

25 worse determination results were found for ENSEMBLE. The FI1_HTAP simulation showed the highest determination values. Thus despite the high underestimation of the AE values, it displayed a good skill in the temporal AE representation.

As mentioned above, a good approach to evaluate the spatial and temporal variability of a variable is PDF. A wide PDF indicates wide variability for the studied variable, and a narrow and low variability. For the AOD representation, all the simulations presented similar PDF to the observed values. The behaviour of all the simulations was similar in winter, spring and

30 autumn; simulations FI1 and IT2 presented higher probabilities for lower AOD values than those observed; ES1 presented higher probabilities for high AOD values than those observed due to the above-explained lack of dust gravitational settling. Finally, IT1 presented the most skilful PDF. Given the probability of obtaining AOD values around 0.5 being higher, the IT2 simulations presented the best skills in summer. One general conclusion was reached from the PDF of the AE values. For this variable, all the simulations in all the studied seasons underestimated temporal and spatial variability.

Atmospheric
Chemistry
and Physics
Discussions

In conclusion, the skills of all the simulations in the AOD representation produced lower errors than in the AE representation. For AOD, low and medium values were well-represented, but high values presented larger errors. High values due to dust were overestimated because of an overestimation in the boundary conditions. The high AOD values due to biomass burning were underestimated, which should be ascribed to an understated injection height of the total biomass burning emissions or directly

5   to underestimated emissions. Other high AOD values were underestimated because the emissions which produced these high values were not considered. The errors in the AOD representation evidenced the strong influence of emissions and boundary conditions in the estimation of aerosol optical properties. Generally speaking, the models' skills to represent the variability of AOD were acceptable. For AE, the SILAM simulation underestimated the observed values and the WRF coupled CAMx simulation and the WRF-Chem simulations were those with the best skills in the representation of this variable. But for all the

10 simulations, the variability of this variable was underestimated.

Following these results, further studies are needed to improve the representation of aerosol optical properties, along with other properties such as atmospheric distribution, hygroscopicity, or the ability to act as cloud condensation nuclei (CCN) and ice nuclei (IN). The matter noted in the representation of aerosol properties can help to gain a better representation of ARI and ACI and aerosol effects on meteorology and climate, and could reduce the grave uncertainty in the estimations of changes in

15 the Earth's radiation budget due to aerosols and clouds.

5   Data availability

The outputs from the simulations can be obtained by emailing to *rbianconi@enviroware.com*. MODIS data are publicly available on the MODIS Atmosphere website (https://modis-atmos.gsfc.nasa.gov/MOD04_L2/acquiring.html).

References

Ackermann, I. J., Hass, H., Memmesheimer, M., Ebel, A., Binkowski, F. S., and Shankar, U.: Modal aerosol dynamics model for Europe: development and first applications, Atmospheric Environment, 32, 2981 – 2999, doi:10.1016/S1352-2310(98)00006-5, 1998.

Ahmadov, R., McKeen, S. A., Robinson, A. L., Bahreini, R., Middlebrook, A. M., de Gouw, J. A., Meagher, J., Hsie, E.-Y., Edgerton, E.,
5   Shaw, S., and Trainer, M.: A volatility basis set model for summertime secondary organic aerosols over the eastern United States in 2006, Journal of Geophysical Research: Atmospheres, 117, doi:10.1029/2011JD016831, d06301, 2012.

Ångström, A.: On the atmospheric transmission of sun radiation and on dust in the air, Geografiska Annaler, 11, 156–166, 1929.

Balzarini, A.: Implementing the WRF-Chem modeling system to investigate the interactions between air quality and meteorology, Ph.D. thesis, University of Milano-Bicocca, 2013.

10 Balzarini, A., Pirovano, G., Honzak, L., Žabkar, R., Curci, G., Forkel, R., Hirtl, M., José, R. S., Tuccella, P., and Grell, G.: WRF-Chem model sensitivity to chemical mechanisms choice in reconstructing aerosol optical properties, Atmospheric Environment, 115, 604 – 619, doi:10.1016/j.atmosenv.2014.12.033, 2015.

Barnard, J. C., Fast, J. D., Paredes-Miranda, G., Arnott, W. P., and Laskin, A.: Technical Note: Evaluation of the WRF-Chem "Aerosol Chemical to Aerosol Optical Properties" Module using data from the MILAGRO campaign, Atmospheric Chemistry and Physics, 10,
15   7325–7340, doi:10.5194/acp-10-7325-2010, 2010.

Baró, R., Lorente-Plazas, R., Montávez, J. P., and Jiménez-Guerrero, P.: Biomass burning aerosol impact on surface winds during the 2010 Russian heat wave, Geophysical Research Letters, doi:10.1002/2016GL071484, 2016GL071484, 2017.

Boucher, O.: Atmospheric Aerosols: Properties and Climate Impacts, Springer, 2015.

Boucher, O., Randall, D., Artaxo, P., Bretherton, C., Feingold, G., Forster, P., Kerminen, V.-M., Kondo, Y., Liao, H., Lohmann, U., Rasch,
20   P., Satheesh, S., Sherwood, S., Stevens, B., and Zhang, X.: Clouds and aerosols, in: Climate change 2013: The physical science basis. Contribution of working group I to the fifth assessment report of the intergovernmental panel on climate change, pp. 571–657, Cambridge University Press, 2013.

Chapman, E. G., Gustafson Jr., W. I., Easter, R. C., Barnard, J. C., Ghan, S. J., Pekour, M. S., and Fast, J. D.: Coupling aerosol-cloud-radiative processes in the WRF-Chem model: Investigating the radiative impact of elevated point sources, Atmospheric Chemistry and Physics, 9,
25   945–964, doi:10.5194/acp-9-945-2009, 2009.

Chin, M., Ginoux, P., Kinne, S., Torres, O., Holben, B. N., Duncan, B. N., Martin, R. V., Logan, J. A., Higurashi, A., and Nakajima, T.: Tropospheric aerosol optical thickness from the GOCART model and comparisons with satellite and Sun photometer measurements, Journal of the Atmospheric Sciences, 59, 461–483, 2002.

Colarco, P., da Silva, A., Chin, M., and Diehl, T.: Online simulations of global aerosol distributions in the NASA GEOS-4
30   model and comparisons to satellite and ground-based aerosol optical depth, Journal of Geophysical Research: Atmospheres, 115, doi:10.1029/2009JD012820, d14207, 2010.

Collins, W. J., Lamarque, J.-F., Schulz, M., Boucher, O., Eyring, V., Hegglin, M. I., Maycock, A., Myhre, G., Prather, M., Shindell, D., and Smith, S. J.: AerChemMIP: Quantifying the effects of chemistry and aerosols in CMIP6, Geoscientific Model Development Discussions, 2016, 1–28, doi:10.5194/gmd-2016-139, 2016.

35 Curci, G., Bieser, J., Im, U., Christensen, J. H., Baró, R., na, L. P.-P., Jiménez-Guerrero, P., Prank, M., Colette, A., García-Vivanco, M., Tucella, P., Manders, A., Toros, H., Sokhi, R., Hogrefe, C., Galmarini, S., Solazzo, E., and Bianconi, R.: Black carbon absorption of

Atmospheric
Chemistry
and Physics
Discussions

solar radiation: combining external and internal mixing assumptions, to be submitted to Atmospheric Chemistry and Physics Discussions, https://www.atmos-chem-phys.net/special_issue390.html, 2017.

de Leeuw, G., Neele, F. P., Hill, M., Smith, M. H., and Vignati, E.: Production of sea spray aerosol in the surf zone, Journal of Geophysical Research: Atmospheres, 105, 29 397–29 409, doi:10.1029/2000JD900549, 2000.

5 Dentener, F., Galmarini, S., Hogrefe, C., Carmichael, G., Law, K., and Denby, B., eds.: Global and regional assessment of intercontinental transport of air pollution: results from HTAP, AQMEII and MICS, Special Issue on Atmospheric Chemistry and Physics, https://www.atmos-chem-phys.net/special_issue390.html, 2015.

Donahue, N. M., Robinson, a. L., Stanier, C. O., and Pandis, S. N.: Coupled partitioning, dilution, and chemical aging of semivolatile organics, Environmental Science and Technology, 40, 2635–2643, doi:10.1021/es052297c, 2006.

10 Eck, T. F., Holben, B. N., Reid, J. S., Dubovik, O., Smirnov, A., O'Neill, N. T., Slutsker, I., and Kinne, S.: Wavelength dependence of the optical depth of biomass burning, urban, and desert dust aerosols, Journal of Geophysical Research: Atmospheres, 104, 31 333–31 349, doi:10.1029/1999JD900923, 1999.

ENVIRON, O.: User's Guide to the Comprehensive Air Quality Model with Extensions Version 5.40, ENVIRON International Corporation, Novato, CA., www.camx.com, 2014.

15 Eyring, V.and Lamarque, J.-F., Hess, P., Arfeuille, F., Bowman, K., Chipperfield, M. P., Duncan, B., Fiore, A., Gettelman, A., Giorgetta, M. A., Granier, C., Hegglin, M., Kinnison, D., Kunze, M., Langematz, U., Luo, B., Martin, R., Matthes, K., Newman, P. A., Peter, T., Robock, A., Ryerson, T., Saiz-Lopez, A., Salawitch, R., Schultz, M., Shepherd, T. G., Shindell, D., Stähelin, J., Tegtmeier, S., Thomason, L., Tilmes, S., Vernier, J.-P., Waugh, D. W., and Young, P. J.: Overview of IGAC/SPARC Chemistry-Climate Model Initiative (CCMI) Community Simulations in Support of Upcoming Ozone and Climate Assessments, SPARC Newsletter, pp. 48–66, 2013.

20 Eyring, V., Bony, S., Meehl, G. A., Senior, C. A., Stevens, B., Stouffer, R. J., and Taylor, K. E.: Overview of the Coupled Model Intercomparison Project Phase 6 (CMIP6) experimental design and organization, Geoscientific Model Development, 9, 1937–1958, doi:10.5194/gmd-9-1937-2016, 2016.

Fast, J. D., Gustafson, W. I., Easter, R. C., Zaveri, R. A., Barnard, J. C., Chapman, E. G., Grell, G. A., and Peckham, S. E.: Evolution of ozone, particulates, and aerosol direct radiative forcing in the vicinity of Houston using a fully coupled meteorology-chemistry-aerosol

25 model, Journal of Geophysical Research: Atmospheres, 111, doi:10.1029/2005JD006721, d21305, 2006.

Forkel, R., Balzarini, A., Baró, R., Bianconi, R., Curci, G., Jiménez-Guerrero, P., Hirtl, M., Honzak, L., Lorenz, C., Im, U., Pérez, J. L., Pirovano, G., José, R. S., Tuccella, P., Werhahn, J., and Źabkar, R.: Analysis of the WRF-Chem contributions to AQMEII phase2 with respect to aerosol radiative feedbacks on meteorology and pollutant distributions, Atmospheric Environment, 115, 630 – 645, doi:10.1016/j.atmosenv.2014.10.056, 2015.

30 Forkel, R., Brunner, D., Baklanov, A., Balzarini, A., Hirtl, M., Honzak, L., Jiménez-Guerrero, P., Jorba, O., Pérez, J., San José, R., et al.: A Multi-model Case Study on Aerosol Feedbacks in Online Coupled Chemistry-Meteorology Models Within the COST Action ES1004 EuMetChem, in: Air Pollution Modeling and its Application XXIV, pp. 23–28, Springer, 2016.

Fuzzi, S., Baltensperger, U., Carslaw, K., Decesari, S., Denier van der Gon, H., Facchini, M. C., Fowler, D., Koren, I., Langford, B., Lohmann, U., Nemitz, E., Pandis, S., Riipinen, I., Rudich, Y., Schaap, M., Slowik, J. G., Spracklen, D. V., Vignati, E., Wild, M., Williams, M., and

35 Gilardoni, S.: Particulate matter, air quality and climate: lessons learned and future needs, Atmospheric Chemistry and Physics, 15, 8217–8299, doi:10.5194/acp-15-8217-2015, 2015.

Galmarini, S., Rao, S. T., and Steyn, D. G.: Preface to the AQMEII p1 Special issue, Atmospheric Enviroment, 53, 1–3, 2012.

Galmarini, S., Hogrefe, C., Brunner, D., Makar, P., and Baklanov, A.: Preface, Atmospheric Environment, pp. 340–344, 2015.

Galmarini, S., Koffi, B., Solazzo, E., Keating, T., Hogrefe, C., Schulz, M., Benedictow, A., Griesfeller, J. J., Janssens-Maenhout, G., Carmichael, G., Fu, J., and Dentener, F.: Technical note: Coordination and harmonization of the multi-scale, multi-model activities HTAP2, AQMEII3, and MICS-Asia3: simulations, emission inventories, boundary conditions, and model output formats, Atmospheric Chemistry and Physics, 17, 1543–1555, doi:10.5194/acp-17-1543-2017, 2017.

5 Ghan, S., Laulainen, N., Easter, R., Wagener, R., Nemesure, S., Chapman, E., Zhang, Y., and Leung, R.: Evaluation of aerosol direct radiative forcing in MIRAGE, Journal of Geophysical Research: Atmospheres, 106, 5295–5316, doi:10.1029/2000JD900502, 2001.

Ginoux, P., Chin, M., Tegen, I., Prospero, J. M., Holben, B., Dubovik, O., and Lin, S.-J.: Sources and distributions of dust aerosols simulated with the GOCART model, Journal of Geophysical Research: Atmospheres, 106, 20 255–20 273, doi:10.1029/2000JD000053, 2001.

Ginoux, P., Horowitz, L. W., Ramaswamy, V., Geogdzhayev, I. V., Holben, B. N., Stenchikov, G., and Tie, X.: Evaluation of aerosol distribu-
10 tion and optical depth in the Geophysical Fluid Dynamics Laboratory coupled model CM2.1 for present climate, Journal of Geophysical Research: Atmospheres, 111, doi:10.1029/2005JD006707, d22210, 2006.

Gong, S. L.: A parameterization of sea-salt aerosol source function for sub- and super-micron particles, Global Biogeochemical Cycles, 17, doi:10.1029/2003GB002079, 1097, 2003.

Grell, G. A., Peckham, S. E., Schmitz, R., McKeen, S. A., Frost, G., Skamarock, W. C., and Eder, B.: Fully coupled "online" chemistry
15 within the WRF model, Atmospheric Environment, 39, 6957 – 6975, doi:10.1016/j.atmosenv.2005.04.027, 2005.

Guenther, C.: Estimates of global terrestrial isoprene emissions using MEGAN (Model of Emissions of Gases and Aerosols from Nature), Atmospheric Chemistry and Physics, 6, 2006.

Hess, M., Koepke, P., and Schult, I.: Optical Properties of Aerosols and Clouds: The Software Package OPAC, Bulletin of the American Meteorological Society, 79, 831–844, 1998.

20 Holben, B., Eck, T., Slutsker, I., Tanre, D., Buis, J., Setzer, A., Vermote, E., Reagan, J., Kaufman, Y., Nakajima, T., et al.: AERONET—A federated instrument network and data archive for aerosol characterization, Remote sensing of environment, 66, 1–16, 1998.

Ignatov, A., Stowe, L., and Singh, R.: Sensitivity study of the Ångström exponent derived from AVHRR over the oceans, Advances in Space Research, 21, 439–442, 1998.

Janssens-Maenhout, G., Crippa, M., Guizzardi, D., Dentener, F., Muntean, M., Pouliot, G., Keating, T., Zhang, Q., Kurokawa, J., Wankmüller,
25 R., Denier van der Gon, H., Kuenen, J. J. P., Klimont, Z., Frost, G., Darras, S., Koffi, B., and Li, M.: HTAP_v2.2: a mosaic of regional and global emission grid maps for 2008 and 2010 to study hemispheric transport of air pollution, Atmospheric Chemistry and Physics, 15, 11 411–11 432, doi:10.5194/acp-15-11411-2015, 2015.

Jeuken, A., Veefkind, J. P., Dentener, F., Metzger, S., and Gonzalez, C. R.: Simulation of the aerosol optical depth over Eu-
rope for August 1997 and a comparison with observations, Journal of Geophysical Research: Atmospheres, 106, 28 295–28 311,
30 doi:10.1029/2001JD900063, 2001.

Kim, S.-W., Heckel, A., Frost, G. J., Richter, A., Gleason, J., Burrows, J. P., McKeen, S., Hsie, E.-Y., Granier, C., and Trainer, M.: NO_2 columns in the western United States observed from space and simulated by a regional chemistry model and their implications for NO_x emissions, Journal of Geophysical Research: Atmospheres, 114, doi:10.1029/2008JD011343, d11301, 2009.

Kinne, S., Lohmann, U., Feichter, J., Schulz, M., Timmreck, C., Ghan, S., Easter, R., Chin, M., Ginoux, P., Takemura, T., Tegen, I., Koch,
35 D., Herzog, M., Penner, J., Pitari, G., Holben, B., Eck, T., Smirnov, A., Dubovik, O., Slutsker, I., Tanre, D., Torres, O., Mishchenko, M., Geogdzhayev, I., Chu, D. A., and Kaufman, Y.: Monthly averages of aerosol properties: A global comparison among models, satellite data, and AERONET ground data, Journal of Geophysical Research: Atmospheres, 108, doi:10.1029/2001JD001253, 4634, 2003.

Kinne, S., Schulz, M., Textor, C., Guibert, S., Balkanski, Y., Bauer, S. E., Berntsen, T., Berglen, T. F., Boucher, O., Chin, M., Collins, W., Dentener, F., Diehl, T., Easter, R., Feichter, J., Fillmore, D., Ghan, S., Ginoux, P., Gong, S., Grini, A., Hendricks, J., Herzog, M., Horowitz, L., Isaksen, I., Iversen, T., Kirkevåg, A., Kloster, S., Koch, D., Kristjansson, J. E., Krol, M., Lauer, A., Lamarque, J. F., Lesins, G., Liu, X., Lohmann, U., Montanaro, V., Myhre, G., Penner, J., Pitari, G., Reddy, S., Seland, O., Stier, P., Takemura, T., and Tie, X.: An

5   AeroCom initial assessment – optical properties in aerosol component modules of global models, Atmospheric Chemistry and Physics, 6, 1815–1834, doi:10.5194/acp-6-1815-2006, 2006.

Kong, X., Forkel, R., Sokhi, R. S., Suppan, P., Baklanov, A., Gauss, M., Brunner, D., Baró, R., Balzarini, A., Chemel, C., Curci, G., Jiménez-Guerrero, P., Hirtl, M., Honzak, L., Im, U., Pérez, J. L., Pirovano, G., José, R. S., Schlünzen, K. H., Tsegas, G., Tuccella, P., Werhahn, J., Żabkar, R., and Galmarini, S.: Analysis of meteorology–chemistry interactions during air pollution episodes using online coupled models

10   within AQMEII phase-2, Atmospheric Environment, 115, 527 – 540, doi:10.1016/j.atmosenv.2014.09.020, 2015.

Kulmala, M., Asmi, A., Lappalainen, H. K., Baltensperger, U., Brenguier, J.-L., Facchini, M. C., Hansson, H.-C., Hov, Ø., O'Dowd, C. D., Pöschl, U., Wiedensohler, A., Boers, R., Boucher, O., de Leeuw, G., Denier van der Gon, H. A. C., Feichter, J., Krejci, R., Laj, P., Lihavainen, H., Lohmann, U., McFiggans, G., Mentel, T., Pilinis, C., Riipinen, I., Schulz, M., Stohl, A., Swietlicki, E., Vignati, E., Alves, C., Amann, M., Ammann, M., Arabas, S., Artaxo, P., Baars, H., Beddows, D. C. S., Bergström, R., Beukes, J. P., Bilde, M., Burkhart, J. F.,

15   Canonaco, F., Clegg, S. L., Coe, H., Crumeyrolle, S., D'Anna, B., Decesari, S., Gilardoni, S., Fischer, M., Fjaeraa, A. M., Fountoukis, C., George, C., Gomes, L., Halloran, P., Hamburger, T., Harrison, R. M., Herrmann, H., Hoffmann, T., Hoose, C., Hu, M., Hyvärinen, A., Hõrrak, U., Iinuma, Y., Iversen, T., Josipovic, M., Kanakidou, M., Kiendler-Scharr, A., Kirkevåg, A., Kiss, G., Klimont, Z., Kolmonen, P., Komppula, M., Kristjánsson, J.-E., Laakso, L., Laaksonen, A., Labonnote, L., Lanz, V. A., Lehtinen, K. E. J., Rizzo, L. V., Makkonen, R., Manninen, H. E., McMeeking, G., Merikanto, J., Minikin, A., Mirme, S., Morgan, W. T., Nemitz, E., O'Donnell, D., Panwar, T. S.,

20   Pawlowska, H., Petzold, A., Pienaar, J. J., Pio, C., Plass-Duelmer, C., Prévôt, A. S. H., Pryor, S., Reddington, C. L., Roberts, G., Rosenfeld, D., Schwarz, J., Seland, Ø., Sellegri, K., Shen, X. J., Shiraiwa, M., Siebert, H., Sierau, B., Simpson, D., Sun, J. Y., Topping, D., Tunved, P., Vaattovaara, P., Vakkari, V., Veefkind, J. P., Visschedijk, A., Vuollekoski, H., Vuolo, R., Wehner, B., Wildt, J., Woodward, S., Worsnop, D. R., van Zadelhoff, G.-J., Zardini, A. A., Zhang, K., van Zyl, P. G., Kerminen, V.-M., S Carslaw, K., and Pandis, S. N.: General overview: European Integrated project on Aerosol Cloud Climate and Air Quality interactions (EUCAARI); integrating aerosol research from nano

25   to global scales, Atmospheric Chemistry and Physics, 11, 13 061–13 143, doi:10.5194/acp-11-13061-2011, 2011.

Landi, T. C.: AODEM, ISBN 10: 3659318027 / ISBN 13: 9783659318023, LAP Lambert Academic Publishing, 2013.

Levy, R., Mattoo, S., Munchak, L., Remer, L., Sayer, A., and Hsu, N.: The Collection 6 MODIS aerosol products over land and ocean, Atmos. Meas. Tech, 6, 2989–3034, 2013.

Liu, X., Easter, R. C., Ghan, S. J., Zaveri, R., Rasch, P., Shi, X., Lamarque, J.-F., Gettelman, A., Morrison, H., Vitt, F., Conley, A., Park,

30   S., Neale, R., Hannay, C., Ekman, A. M. L., Hess, P., Mahowald, N., Collins, W., Iacono, M. J., Bretherton, C. S., Flanner, M. G., and Mitchell, D.: Toward a minimal representation of aerosols in climate models: description and evaluation in the Community Atmosphere Model CAM5, Geoscientific Model Development, 5, 709–739, doi:10.5194/gmd-5-709-2012, 2012.

Makar, P., Gong, W., Hogrefe, C., Zhang, Y., Curci, G., Żabkar, R., Milbrandt, J., Im, U., Balzarini, A., Baró, R., Bianconi, R., Cheung, P., Forkel, R., Gravel, S., Hirtl, M., Honzak, L., Hou, A., Jiménez-Guerrero, P., Langer, M., Moran, M., Pabla, B., Pérez, J., Pirovano,

35   G., José, R. S., Tuccella, P., Werhahn, J., Zhang, J., and Galmarini, S.: Feedbacks between air pollution and weather, part 2: Effects on chemistry, Atmospheric Environment, 115, 499 – 526, doi:10.1016/j.atmosenv.2014.10.021, 2015.

Moorthy, K. K., Satheesh, S. K., Babu, S. S., and Dutt, C. B. S.: Integrated Campaign for Aerosols, gases and Radiation Budget (ICARB): An overview, Journal of Earth System Science, 117, 243–262, doi:10.1007/s12040-008-0029-7, 2008.

Ogren, J.: WMO/GAW Standard Operating Procedures for In-Situ Measurements of Aerosol Mass Concentration, Light Scattering and Light Absorption, WMO/GAW, Tech. rep., World Meteorological Organization Report, 2011.

Palacios-Peña, L., Baró, R., Baklanov, A., Balzarini, A., Brunner, D., Forkel, R., Hirtl, M., Honzak, L., López-Romero, J. M., Pérez, J. L., Pirovano, G., San José, R., Schröder, W., Werhahn, J., Wolke, R., Zabkar, R., and Jiménez-Guerrero, P.: An assessment of aerosol optical
5   properties from remote sensing observations and regional chemistry-climate coupled models over Europe, Atmospheric Chemistry and Physics Discussions, 2017, 1–37, doi:10.5194/acp-2017-877, https://www.atmos-chem-phys-discuss.net/acp-2017-877/, 2017a.

Palacios-Peña, L., Baró, R., Guerrero-Rascado, J. L., Alados-Arboledas, L., Brunner, D., and Jiménez-Guerrero, P.: Evaluating the representation of aerosol optical properties using an online coupled model over the Iberian Peninsula, Atmospheric Chemistry and Physics, 17, 277–296, doi:10.5194/acp-17-277-2017, 2017b.

10 Paredes-Miranda, G., Arnott, W. P., Jimenez, J. L., Aiken, A. C., Gaffney, J. S., and Marley, N. A.: Primary and secondary contributions to aerosol light scattering and absorption in Mexico City during the MILAGRO 2006 campaign, Atmospheric Chemistry and Physics, 9, 3721–3730, doi:10.5194/acp-9-3721-2009, 2009.

Pouliot, G., Pierce, T., van der Gon, H. D., Schaap, M., Moran, M., and Nopmongcol, U.: Comparing emission inventories and model-ready emission datasets between Europe and North America for the AQMEII project, Atmospheric Environment, 53, 4–14, 2012.

15 Pouliot, G., van der Gon, H. A. D., Kuenen, J., Zhang, J., Moran, M. D., and Makar, P. A.: Analysis of the emission inventories and model-ready emission datasets of Europe and North America for phase 2 of the AQMEII project, Atmospheric Environment, 115, 345–360, 2015.

Poupkou, A., Giannaros, T., Markakis, K., Kioutsioukis, I., Curci, G., Melas, D., and Zerefos, C.: A model for European biogenic volatile organic compound emissions: software development and first validation, Environmental Modelling & Software, 25, 1845–1856, 2010.

20 Randall, D. A., Wood, R. A., Bony, S., Colman, R., Fichefet, T., Fyfe, J., Kattsov, V., Pitman, A., Shukla, J., Srinivasan, J., Stouffer, R. J., Sumi, A., and Taylor, K. E.: Climate models and their evaluation, in: Climate change 2007: The physical science basis. Contribution of Working Group I to the Fourth Assessment Report of the IPCC (FAR), pp. 589–662, Cambridge University Press, 2007.

Rao, S. T., Galmarini, S., and Puckett, K.: Air Quality Model Evaluation International Initiative (AQMEII): Advancing the State of the Science in Regional Photochemical Modeling and Its Applications, Bulletin of the American Meteorological Society, 92, 23–30,
25   doi:10.1175/2010BAMS3069.1, 2011.

Reddy, M. S., Boucher, O., Bellouin, N., Schulz, M., Balkanski, Y., Dufresne, J.-L., and Pham, M.: Estimates of global multicomponent aerosol optical depth and direct radiative perturbation in the Laboratoire de Météorologie Dynamique general circulation model, Journal of Geophysical Research: Atmospheres, 110, doi:10.1029/2004JD004757, d10S16, 2005.

Remer, L. A., Kaufman, Y., Tanré, D., Mattoo, S., Chu, D., Martins, J. V., Li, R.-R., Ichoku, C., Levy, R., Kleidman, R., Eck, T. F., E, V., and
30   Holben, B. N.: The MODIS aerosol algorithm, products, and validation, Journal of the atmospheric sciences, 62, 947–973, 2005.

Schell, B., Ackermann, I. J., Hass, H., Binkowski, F. S., and Ebel, A.: Modeling the formation of secondary organic aerosol within a comprehensive air quality model system, Journal of Geophysical Research: Atmospheres, 106, 28 275–28 293, doi:10.1029/2001JD000384, 2001.

Schulz, M., Chin, M., and Kinne, S.: The aerosol model comparison project, AeroCom, phase II: Clearing up diversity, IGAC Newsletter,
35   2009.

Shaw, W. J., Allwine, K. J., Fritz, B. G., Rutz, F. C., Rishel, J. P., and Chapman, E. G.: An evaluation of the wind erosion module in DUSTRAN, Atmospheric Environment, 42, 1907 – 1921, doi:https://doi.org/10.1016/j.atmosenv.2007.11.022, 2008.

Soares, J., Sofiev, M., and Hakkarainen, J.: Uncertainties of wild-land fires emission in AQMEII phase 2 case study, Atmospheric Environment, 115, 361–370, 2015.

Sofiev, M.: A model for the evaluation of long-term airborne pollution transport at regional and continental scales, Atmospheric Environment, 34, 2481–2493, 2000.

5 Sofiev, M., Soares, J., Prank, M., de Leeuw, G., and Kukkonen, J.: A regional-to-global model of emission and transport of sea salt particles in the atmosphere, Journal of Geophysical Research: Atmospheres, 116, 2011.

Sofiev, M., Vira, J., Kouznetsov, R., Prank, M., Soares, J., and Genikhovich, E.: Construction of the SILAM Eulerian atmospheric dispersion model based on the advection algorithm of Michael Galperin, Geoscientific Model Development, 8, 3497–3522, doi:10.5194/gmd-8-3497-2015, 2015.

10 Solazzo, E., Bianconi, R., Pirovano, G., Matthias, V., Vautard, R., Moran, M. D., Appel, K. W., Bessagnet, B., Brandt, J., Christensen, J. H., Chemel, C., Coll, I., Ferreira, J., Forkel, R., Francis, X. V., Grell, G., Grossi, P., Hansen, A. B., Miranda, A. I., Nopmongcol, U., Prank, M., Sartelet, K. N., Schaap, M., Silver, J. D., Sokhi, R. S., Vira, J., Werhahn, J., Wolke, R., Yarwood, G., Zhang, J., Rao, S. T., and Galmarini, S.: Operational model evaluation for particulate matter in Europe and North America in the context of AQMEII, Atmospheric Environment, 53, 75 – 92, doi:10.1016/j.atmosenv.2012.02.045, 2012.

15 Solazzo, E., Galmarini, S., Bianconi, R., and Rao, S. T.: Model evaluation for surface concentration of particulate matter in Europe and North America in the context of AQMEII, in: Air Pollution Modeling and its Application XXII, pp. 375–379, Springer, 2014.

Solazzo, E., Bianconi, R., Hogrefe, C., Curci, G., Tuccella, P., Alyuz, U., Balzarini, A., Baró, R., Bellasio, R., Bieser, J., Brandt, J., Christensen, J. H., Colette, A., Francis, X., Fraser, A., Vivanco, M. G., Jiménez-Guerrero, P., Im, U., Manders, A., Nopmongcol, U., Kitwiroon, N., Pirovano, G., Pozzoli, L., Prank, M., Sokhi, R. S., Unal, A., Yarwood, G., and Galmarini, S.: Evaluation and error apportionment of an ensemble of atmospheric chemistry transport modeling systems: multivariable temporal and spatial breakdown, Atmospheric Chemistry and Physics, 17, 3001–3054, doi:10.5194/acp-17-3001-2017, 2017.

Solmon, F., Giorgi, F., and Liousse, C.: Aerosol modelling for regional climate studies: application to anthropogenic particles and evaluation over a European/African domain, Tellus B, 58, 51–72, 2006.

Stockwell, W. R., Middleton, P., Chang, J. S., and Tang, X.: The second generation regional acid deposition model chemical mechanism for regional air quality modeling, Journal of Geophysical Research: Atmospheres, 95, 16 343–16 367, doi:10.1029/JD095iD10p16343, 1990.

Toll, V., Reis, K., Ots, R., Kaasik, M., Männik, A., Prank, M., and Sofiev, M.: SILAM and MACC reanalysis aerosol data used for simulating the aerosol direct radiative effect with the NWP model HARMONIE for summer 2010 wildfire case in Russia, Atmospheric Environment, 121, 75–85, doi:10.1016/j.atmosenv.2015.06.007, 2015a.

Toll, V., Reis, K., Ots, R., Kaasik, M., Männik, A., Prank, M., and Sofiev, M.: SILAM and MACC reanalysis aerosol data used for simulating the aerosol direct radiative effect with the NWP model HARMONIE for summer 2010 wildfire case in Russia, Atmospheric Environment, 121, 75–85, 2015b.

Tørseth, K., Aas, W., Breivik, K., Fjæraa, A., Fiebig, M., Hjellbrekke, A., Lund Myhre, C., Solberg, S., and Yttri, K.: Introduction to the European Monitoring and Evaluation Programme (EMEP) and observed atmospheric composition change during 1972–2009, Atmospheric Chemistry and Physics, 12, 5447–5481, 2012.

35 Tuccella, P., Curci, G., Visconti, G., Bessagnet, B., Menut, L., and Park, R. J.: Modeling of gas and aerosol with WRF/Chem over Europe: Evaluation and sensitivity study, Journal of Geophysical Research: Atmospheres, 117, 2012.

Atmospheric
Chemistry
and Physics
Discussions

Tuccella, P., Curci, G., Grell, G. A., Visconti, G., Crumeyrolle, S., Schwarzenboeck, A., and Mensah, A. A.: A new chemistry option in WRF-Chem v. 3.4 for the simulation of direct and indirect aerosol effects using VBS: evaluation against IMPACT-EUCAARI data, Geoscientific Model Development, 8, 2749–2776, doi:10.5194/gmd-8-2749-2015, 2015.

Wang, K., Yahya, K., Zhang, Y., Hogrefe, C., Pouliot, G., Knote, C., Hodzic, A., José, R. S., Pérez, J. L., Jiménez-Guerrero, P., Baró, R., Makar, P., and Bennartz, R.: A multi-model assessment for the 2006 and 2010 simulations under the Air Quality Model Evaluation International Initiative (AQMEII) Phase 2 over North America: Part II. Evaluation of column variable predictions using satellite data, Atmospheric Environment, 115, 587 – 603, doi:10.1016/j.atmosenv.2014.07.044, 2015.

Warneke, C., Froyd, K. D., Brioude, J., Bahreini, R., Brock, C. A., Cozic, J., de Gouw, J. A., Fahey, D. W., Ferrare, R., Holloway, J. S., Middlebrook, A. M., Miller, L., Montzka, S., Schwarz, J. P., Sodemann, H., Spackman, J. R., and Stohl, A.: An important contribution to springtime Arctic aerosol from biomass burning in Russia, Geophysical Research Letters, 37, doi:10.1029/2009GL041816, l01801, 2010.

Weil, J., Sykes, R., and Venkatram, A.: Evaluating air-quality models: review and outlook, Journal of Applied Meteorology, 31, 1121–1145, 1992.

Willmott, C. J. and Matsuura, K.: Advantages of the mean absolute error (MAE) over the root mean square error (RMSE) in assessing average model performance, Climate research, 30, 79, 2005.

Willmott, C. J., Ackleson, S. G., Davis, R. E., Feddema, J. J., Klink, K. M., Legates, D. R., O'Donnell, J., and Rowe, C. M.: Statistics for the evaluation and comparison of models, Journal of Geophysical Research: Oceans, 90, 8995–9005, doi:10.1029/JC090iC05p08995, 1985.

Winker, D. M., Pelon, J. R., and McCormick, M. P.: The CALIPSO mission: Spaceborne lidar for observation of aerosols and clouds, in: Third International Asia-Pacific Environmental Remote Sensing Remote Sensing of the Atmosphere, Ocean, Environment, and Space, pp. 1–11, International Society for Optics and Photonics, 2003.

Wooster, M. J., Roberts, G., Perry, G., and Kaufman, Y.: Retrieval of biomass combustion rates and totals from fire radiative power observations: FRP derivation and calibration relationships between biomass consumption and fire radiative energy release, Journal of Geophysical Research: Atmospheres, 110, 2005.

Zhang, K., O'Donnell, D., Kazil, J., Stier, P., Kinne, S., Lohmann, U., Ferrachat, S., Croft, B., Quaas, J., Wan, H., Rast, S., and Feichter, J.: The global aerosol-climate model ECHAM-HAM, version 2: sensitivity to improvements in process representations, Atmospheric Chemistry and Physics, 12, 8911–8949, doi:10.5194/acp-12-8911-2012, 2012.